AD-A150 792   LOCAL COVARIANCE FUNCTIONS AND DENSITY DISTRIBUTIONS   1/1
              (U) OHIO STATE UNIV RESEARCH FOUNDATION COLUMBUS
              R FORSBERG JUN 84 OSU/DGSS-356 AFGL-TR-84-0214
UNCLASSIFIED F19628-82-K-0022   F/G 8/5   NL
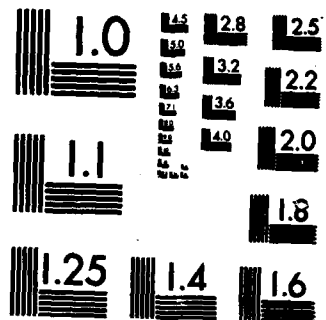
END
FILMED

DTIC

MICROCOPY RESOLUTION TEST CHART
NATIONAL BUREAU OF STANDARDS-1963-A

AFGL-TR-84-0214

LOCAL COVARIANCE FUNCTIONS AND DENSITY DISTRIBUTIONS

Rene Forsberg

The Ohio State University
Research Foundation
Columbus, Ohio 43212

June, 1984

Scientific Report No. 6
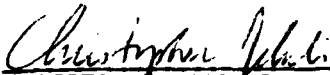
Approved for public release; distribution unlimited

AIR FORCE GEOPHYSICS LABORATORY
AIR FORCE SYSTEMS COMMAND
UNITED STATES AIR FORCE
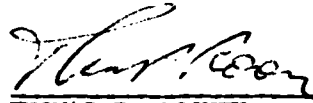HANSCOM AFB, MASSACHUSETTS 01731

AD-A150 792

DTIC FILE COPY

DTIC
ELECTE
MAR 0 1 1985
E

CONTRACTOR REPORTS

This technical report has been reviewed and is approved for publication.

CHRISTOPHER JEKELI
Contract Manager

THOMAS P. ROONEY
Chief, Geodesy & Gravity Branch

FOR THE COMMANDER

DONALD H. ECKHARDT
Director
Earth Sciences Division

This report has been reviewed by the ESD Public Affairs Office (PA) and is releasable to the National Technical Information Service (NTIS).

Qualified requesters may obtain additional copies from the Defense Technical Information Center. All others should apply to the National Technical Information Service.

If your address has changed, or if you wish to be removed from the mailing list, or if the addressee is no longer employed by your organization, please notify AFGL/DAA, Hanscom AFB, MA 01731. This will assist us in maintaining a current mailing list.

REPORT DOCUMENTATION PAGE		READ INSTRUCTIONS BEFORE COMPLETING FORM
1. REPORT NUMBER AFGL-TR-84-0214	**2. GOVT ACCESSION NO.**	**3. RECIPIENT'S CATALOG NUMBER**
4. TITLE (and Subtitle) Local Covariance Functions and Density Distributions		**5. TYPE OF REPORT & PERIOD COVERED** Scientific Report No. 6
		6. PERFORMING ORG. REPORT NUMBER OSU/DGSS-356
7. AUTHOR(s) Rene Forsberg		**8. CONTRACT OR GRANT NUMBER(s)** F19628-82-K-0022
9. PERFORMING ORGANIZATION NAME AND ADDRESS The Ohio State University Research Foundation 1958 Neil Avenue, Columbus, Ohio 43210		**10. PROGRAM ELEMENT, PROJECT, TASK AREA & WORK UNIT NUMBERS** 61102F 2309G1BC
11. CONTROLLING OFFICE NAME AND ADDRESS Air Force Geophysics Laboratory Hanscom AFB, Massachusetts 01731 Monitor/Christopher Jekeli/LWG		**12. REPORT DATE** June 1984
		13. NUMBER OF PAGES 56
14. MONITORING AGENCY NAME & ADDRESS(if different from Controlling Office)		**15. SECURITY CLASS. (of this report)** Unclassified
		15a. DECLASSIFICATION/DOWNGRADING SCHEDULE

16. DISTRIBUTION STATEMENT (of this Report)

Approved for public release; distribution unlimited

17. DISTRIBUTION STATEMENT (of the abstract entered in Block 20, if different from Report)

18. SUPPLEMENTARY NOTES

from back p.

19. KEY WORDS (Continue on reverse side if necessary and identify by block number)

Originator-supplied keywords included:

Gravity, Covariance Functions, Density Distributions, Collocation,

20. ABSTRACT (Continue on reverse side if necessary and identify by block number)

The relationship between covariance functions and the density anomaly distributions generating the gravity field is studied using the ensemble averaging theorem, yielding interpretations of common well-known covariance functions in terms of simplified statistical mass models.

Emphasis is on application for local gravity field modelling (e.g. assuming a high degree-and-order spherical harmonic reference field to be used), within the framework of the planar approximation. The very simple rela-

DD FORM 1473 1 JAN 73   EDITION OF 1 NOV 65 IS OBSOLETE

—➤tionship existing between the planar power spectrum and the degree variances are treated in detail, and it is outlined how the shape of the power spectrum may be used as a geophysical inversion tool, to yield depths to density contrast interfaces within the earth.

As a special application of the simple covariance functions associated with statistical mass distributions, it is shown how least-squares collocation may be interpreted as generalized point mass modelling.

Finally, formulas are given for practically applicable local multi-layer covariance models ("compensated Poisson model"), and gravity anomalies in a number of sample areas in the United States are analyzed to yield empirical covariance functions, power spectra and degree-variances. Multi-layer covariance models are given for each area, yielding quite similar results, and demonstrating the generally logarithmic decay ($\sim \ell^{-3}$) of the degree variances, even for degrees up to $\ell = 5400$.

to last p.

FOREWORD

Accession For	
NTIS GRA&I	☒
DTIC TAB	☐
Unannounced	☐
Justification	

By
Distribution/
Availability Codes

Dist	Avail and/or Special
A-1	

DTIC
COPY
INSPECTED
1

Contents

1. Introduction

Covariance functions for the gravity field form the basis for optimal gravity field approximation techniques such as collocation and Wiener filtering, and are also indispensable for error studies and similar topics relating to integral formulas etc. Considering collocation, it is generally stated that the result of application of collocation techniques is insensitive to the actual choice of covariance function parameters, whereas the error estimates are critically dependent on these parameters. This is a somewhat dangerous statement: experience has shown it indeed to be the case for e.g. gravity interpolation, but when predicting a different "order" of gravity field quantities, e.g. geoid undulations from gravity, it is definitely not the case: the predicted geoid may be too rough or too smooth depending on whether the implied covariance model has too much or too little power in the longer wavelengths.

There is therefore a definite need for "good" covariance models, i.e. parametrical models giving a good fit to empirical data from a given area. Many "simple" models for parametric covariance functions have been suggested and evaluated over the years; for a review see e.g. Moritz (1980). Possible misfits of the "simple" models may be reduced by "multiple" models, as e.g. suggested by Jekeli (1978), Jordan (1978) and many others. These simple and improved covariance models may be interpreted in terms of statistical properties of the <u>density anomalies</u> generating the anomalous gravity field. In the author's opinion, such interpretation models, outlined in the sequel, will principally be of value in clarifying the relationship between the various types of simple covariance models in use, and for providing geophysically reasonable improved covariance function models.

Another - and very important application - is the use of "covariance interpretation" as a geophysical exploration method, to obtain depths to density anomalies. Such statistical methods have been dominating in potential field geophysics for the last decade or so, and have been applied successfully and routinely for aeromagnetic data. For gravity, however, the successes have been more limited, reflecting partly the usually much less dense gravity coverage available and - especially - that the sources of the gravity field variations are more "spread out" and less applicable for the "white noise layer" descriptions which magnetic sources often seem to follow, e.g. when unmagnetic sediments are overlying a crystalline basement.

In the sequel, the relationship between "statistical" density anomaly distributions and associated covariance functions will be outlined. As a supplemental remark, the formulation expressing collocation as simple generalized point mass modeling will be mentioned, pointing out the simple relationship existing between collocation and geophysical inversion techniques. Through the use of such geophysical-oriented approaches I think that some of the basics of collocation are "demystified", giving e.g. physical significance to such things as the depth to the Bjerhammar sphere.

In this presentation, I will focus on local covariance functions, applicable only for a given area or geologic province. Certainly the earth's gravity field is in no way a stationary process, and local empirical covariance must be used as a guideline for choosing optimum parametric covariance models (or, rather, the "best" Hilbert space kernels) for such an area. For local applications, global information available through spherical harmonic expansions should always be utilized by subtracting such a reference field. The remaining "residual" field will have less variance and shorter correlation length, and especially when using the available high degree-and-order expansions complete to degree 180 (e.g. "Rapp-180", Rapp 1981) the "variations" will be so local, that the flat-earth approximation becomes completely justifiable.

This planar approximation will be the object for the present work. To exaggerate: by the excellent spherical harmonic models now available, only local problems remain in physical geodesy! And locally everybody knows the earth is flat. In the planar approximation, the discrete spherical harmonic spectrum will be replaced by the continuous Fourier spectrum. Although no simple transition exists between these spectra, a remarkably simple and accurate transition exists between the power spectrum and the degree-variances. This simple relationship will be treated in some detail in the next section. Due to this simple relationship, results for the planar approximation given in the sequel are more or less directly transferrable to a spherical earth.

At the end of the report, some results for actual data in the U.S. will be used as illustrations, to show some of the applications and limitations of the simple covariance models and implied density anomaly distributions,and to compare the "local" results to conventional global covariance functions.

2. Spectral Analysis of Covariance Functions

The anomalous potential of the earth defined as the difference between the actual geopotential W and a normal "ellipsoidal" potential U, may be expanded in fully normalized spherical harmonics as

$$T(r, \phi, \lambda) = \sum_{\ell=2}^{\infty} \sum_{m=-\ell}^{\ell} \bar{a}_{\ell m}(\frac{R}{r})^{\ell+1}\bar{Y}_{\ell m}(\phi, \lambda), \quad \bar{Y}_{\ell m}(\phi, \lambda) = \begin{cases} \bar{P}_{\ell m}(\sin\phi)\cos m\lambda & (m \geq 0) \\ \\ P_{\ell m}(\sin\phi)\sin m\lambda & (m < 0) \end{cases} \quad (2.1)$$

The function T will be harmonic ($\nabla^2 T=0$) outside a sphere of radius R, usually taken as a mean earth radius in available solutions. The spherical harmonic "power spectrum" is the well-known degree-variances

$$\sigma_\ell = \sum_{m=-\ell}^{\ell} \bar{a}_{\ell m}^2 \qquad (2.2)$$

If the covariance function K of T is assumed to be isotropic, $K(P,Q)=K(\psi, r_P, r_Q)$, we have the following well-known expression for the spatial covariances

$$K(P, Q) = \sum_{\ell=2}^{\infty} \sigma_\ell \left[\frac{R^2}{r_P r_Q}\right]^{\ell+1} P_\ell(\cos\psi) \qquad (2.3)$$

see e.g. Moritz (1980). On the reference sphere, K and σ_ℓ are thus related by a Legendre transform, and

$$\sigma_\ell = \frac{2\ell+1}{2} \int_0^\pi K(\psi) P_\ell(\cos\psi) \sin\psi d\psi \qquad (2.4)$$

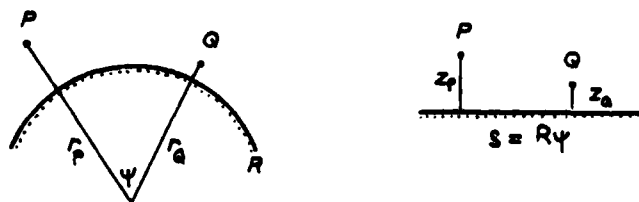Figure 1

The terms K and σ_ℓ relate to the anomalous potential T, and thus by division with normal gravity γ to the height anomaly (spatial geoid undulation) ζ

$$\zeta = \zeta(r, \phi, \lambda) = \frac{T}{\gamma} \tag{2.5}$$

For gravity anomalies

$$\Delta g = -\frac{\partial T}{\partial r} - \frac{2}{r}T = L_{\Delta g}(T) \tag{2.6}$$

similarly C and c_ℓ are traditionally used for covariance function and degree-variances respectively.

C may be expressed by K using covariance propagation:

$$C(P, Q) = L_{\Delta g}^{(P)} L_{\Delta g}^{(Q)} K(\cdot, \cdot) \tag{2.7}$$

where the dots indicate that the gravity anomaly operators $L_{\Delta g}$ should be applied each to one of the variables in K(P, Q). In the spectral domain, the eigenvalue of operator (2.6) is well known to be $\frac{\ell-1}{R}$ (Heiskanen and Moritz, 1967, p. 97), i.e. for the spherical harmonic coefficients

$$\Delta g_{\ell m} = \frac{\ell-1}{R} T_{\ell m} \tag{2.8}$$

and thus

$$c_\ell = \frac{(\ell-1)^2}{R^2} \sigma_\ell \tag{2.9}$$

2.1 The Planar Approximation

The previous topics should be familiar to most geodesists. Less familiar is often the use of Fourier transformations. The Fourier techniques have as advantages their mathematical simplicity, and for practical applications, the efficient transformations algorithms available thorugh FFT - Fast Fourier Transform.

The drawback is that they can only be used <u>locally</u>, since the flat-earth approximation forms the basis. However, with the available high-degree and order spherical harmonic expansions of the geopotential complete to degree 180, (e.g. Rapp, 1981), the <u>residual</u> field

$$T' = T - T_{180 \times 180} \qquad (2.10)$$

may be very suitable for flat-earth methods: T' will have a covariance function of short correlation length (typically 30-50 km), much smaller than distances in which earth curvature effects need be taken into account.

In the flat-earth <u>planar approximation</u> the reference sphere will be replaced by a tangential plane π. An XYZ-system will be used in π, with X positive east, Y positive north and Z positive upwards (Figure 1). The Fourier transformation pair is defined through

$$\tilde{T}(u, v, z) = \int_{\pi} T(x, y, z)e^{-i(ux+vy)}dxdy$$

$$\qquad (2.11)$$

$$T(x, y, z) = \frac{1}{4\pi^2} \int_{\tilde{\pi}} \tilde{T}(u, v, z)e^{i(ux+vy)}dudv$$

where the spatial frequencies or wave numbers will be termed (u, v) in this report, in accordance with the notation of Papoulis (1968). The spectra at various altitudes z are related through

$$\tilde{T}(u, v, z) = \tilde{T}(u, v)e^{-\omega z}, \qquad \omega = \sqrt{u^2+v^2} \qquad (2.12)$$

where $\tilde{T}(u, v)$ is the spectrum at the reference plane π and ω the so-called radial wave number.

Spectra of other gravity field quantities are easily found from their "defining" operators e.g.

∘Gravity anomalies $\quad \Delta g = -\frac{\partial T}{\partial r} - \frac{2}{r}T: \qquad \Delta \tilde{g} = (-\omega - \frac{2}{r})\tilde{T} \approx -\omega\tilde{T}$ (2.13)

∘N-S deflections $\quad \xi = -\frac{1}{\gamma R}\frac{\partial T}{\partial \phi}: \qquad \tilde{\xi} = -\frac{iv}{\gamma}\tilde{T}$ (2.14)

∘E-W deflections $\quad n = -\frac{1}{\gamma \cos\phi\ R}\frac{\partial T}{\partial \lambda}: \qquad \tilde{n} = -\frac{iu}{\gamma}\tilde{T}$ (2.15)

The second term in (2.13) - the "indirect" effect - may often be neglected when using a 180x180 reference field: typical errors for the reference field are at most a few meters in ζ, corresponding to a residual indirect effect of a fraction of a mgal. In this case, an important relationship between the variances of deflections and gravity may be derived. For an arbitrary function f Parsevals equation says

$$\int_{\Pi} f^2(x,\ y)\ dxdy = \frac{1}{4\pi^2}\int_{\tilde{\Pi}} \tilde{f}^2(u,\ v)\ dudv \qquad (2.16)$$

In terms of variance, we have for centered quantities

$$\sigma^2_{\Delta g} = E\{\Delta g^2\} = \frac{1}{4\pi^2} E\{\Delta\tilde{g}^2\} = \frac{1}{4\pi^2}\omega^2\ E\{\tilde{T}^2\} \qquad (2.17)$$

$$\sigma^2_{\xi} + \sigma^2_{n} = \frac{1}{4\pi^2}\left(\frac{u^2}{\gamma^2} + \frac{v^2}{\gamma^2}\right) E\{\tilde{T}^2\} = \frac{1}{4\pi^2}\frac{\omega^2}{\gamma^2} E\{\tilde{T}^2\} = \frac{1}{\gamma^2}\sigma^2_{\Delta g} \qquad (2.18)$$

For an isotropic field $\sigma^2_{\xi}=\sigma^2_{n}$, and thus $\sigma^2_{\xi}=\frac{1}{2\gamma^2}\sigma^2_{\Delta g}$, in terms of r.m.s. variation corresponding to c. 6.7 mgal/arcsec.

2.2 Hankel Transforms

When Fourier analyzing radially symmetric functions, so-called Hankel transforms are obtained.

Let $f(s) = f(x,\ y)$, $s = \sqrt{x^2+y^2}$ be a radially symmetric function in Π. Then the Hankel transform pair is (Papoulis, 1968):

$$\bar{f}(\omega) = \int_0^\infty s f(s) J_0(\omega s) ds \tag{2.19}$$

$$f(s) = \int_0^\infty \omega \bar{f}(\omega) J_0(\omega s) d\omega \tag{2.20}$$

where $J_0(\cdot)$ is the Bessel function of order zero, the Hankel transform and the Fourier transform of f being essentially equivalent since

$$\tilde{f}(u, v) = 2\pi \bar{f}(\omega), \qquad \omega = \sqrt{u^2 + v^2} \tag{2.21}$$

To give two important examples of Hankel transforms, consider the reciprocal distance function $\frac{1}{r} = (x^2 + y^2 + z^2)^{-\frac{1}{2}}$. The transform pairs

$$\frac{1}{r} \longleftrightarrow \frac{1}{\omega} e^{-\omega z} \tag{2.22}$$

$$\frac{1}{r^3} \longleftrightarrow \frac{1}{z} e^{-\omega z} \tag{2.23}$$

may e.g. be found in (Papoulis, 1968, p. 145).

For practical computations, efficient numerical algorithms ("Fast Hankel Transform") exist , building on completely different principles than the FFT-algorithm (Johansen and Sørensen, 1979).

2.3 Covariance Function and Power Spectrum

In the planar approximation the spatial covariance function K becomes a function defined in the space above the reference plane Π:

$$K(\psi, r_P, r_Q) \cong K(s, z_1, z_2) \tag{2.24}$$

where $s = \psi R$ is the distance in the plane. Consider for a moment the covariance function at the reference level $r_P = r_Q = R$, $z_P = z_Q = 0$. The discrete degree-variance spectrum (2.2) will in the planar case be replaced by a continuous function - the **power spectrum** (or rather power spectral density - psd)

$$\phi_{TT}(u, v) = E\{\tilde{T}(u, v)^2\} = \tilde{k}(u, v) \tag{2.25}$$

The power spectrum and covariance function are thus related through a Hankel transform when the covariance function is assumed to be isotropic

$$\phi_{TT}(\omega) = 2\pi\overline{K(s)} = 2\pi\overline{K(\psi R)} \tag{2.26}$$

Spatial covariance expressions, corresponding to (2.3), may be obtained using the upward continuation operator $e^{-\omega z}$ twice:

$$K(s, z_P, z_Q) = \frac{1}{2\pi} \int_0^\infty \omega\phi_{TT}(\omega)e^{-\omega(z_P+z_Q)}J_0(s\omega)d\omega \tag{2.27}$$

see e.g. Nash and Jordan (1978).

2.4 Relationship Between Degree-Variances and the Power Spectrum

A unique and simple relationship exists between the spherical harmonic degree-variances and the flat-earth power spectrum. This relationship, which says that the degree-variances and the power spectrum are more or less the same, have been given e.g. by Dorman and Lewis (1970), in a form slightly different than the one given below.

Consider a local covariance function $K(s)$, where s is the distance. The power spectrum is

$$\phi_{TT}(\omega) = 2\pi\overline{K}(s) = 2\pi \int_0^\infty sK(s)J_0(\omega s)ds \tag{2.28}$$

while the corresponding degree-variances are by (2.4)

$$\sigma_\ell = \frac{2\ell+1}{2} \int_0^\infty K(\psi R) \, P_\ell(\cos\psi)\sin\psi d\psi \tag{2.29}$$

where the covariance function is now viewed as a function of s rather than ψ. However, for a <u>local</u> covariance function, obtained e.g. when a reference field has been subtracted, the function $K(\psi R)$ will be virtually zero for large distances. We may therefore approximate $\sin \psi \doteq \psi$, and obtain

$$\sigma_\ell = \frac{2\ell+1}{2} \int_0^\infty K(\psi R) \ P_\ell(\cos \psi)\psi d\psi \qquad (2.30)$$

The function K has here formally been extended to infinity. Now (2.30) is transformed using the asymptotic expansion of Legendre functions in terms of Bessel functions (Gradstein and Ryshik, 1965, 8.722)

$$P_\ell(\cos \psi) = J_0((2\ell+1) \sin \tfrac{\psi}{2}) + O(\psi^2) \doteq J_0(\tfrac{2\ell+1}{2} \psi) \qquad (2.31)$$

This approximation is valid with high accuracy, even for relatively low degrees and large distances. For example $\ell=10$, $\psi=8.1°$ we have

$$P_\ell(\cos \psi) \quad = 0.5201$$

$$J_0(\tfrac{2\ell+1}{2} \psi) \quad = 0.5196$$

giving only a relative error of 1%.

By insertion of (2.31) into (2.30) then

$$\sigma_\ell = \frac{2\ell+1}{2} \int_0^\infty K(\psi R) J_0(\tfrac{2\ell+1}{2} \psi)\psi d\psi \qquad (2.32)$$

$$= \frac{2\ell+1}{2} \frac{1}{R^2} \int_0^\infty K(s) J_0(\tfrac{2\ell+1}{2} \tfrac{1}{R} s)s ds \qquad (2.33)$$

$$= (\ell+ \tfrac{1}{2}) \frac{1}{R^2} \frac{1}{2\pi} \phi_{TT} (\tfrac{\ell+\frac{1}{2}}{R}) \qquad (2.34)$$

Thus, the degree-variances are obtained essentially simply by multiplying the power spectrum by ℓ, at the "natural" wave numbers $\omega_\ell = \frac{\ell+\frac{1}{2}}{R}$

Therefore, results derived in the sequel for the power spectra of various density distributions and masses may be directly transformed into "spherical" results, especially since the emphasis here is on <u>local</u> phenomena. As seen from the numerical example, the derived degree-variances may be sufficiently accurate even as far down as $\ell=10$.

3. The Relationship Between Covariance Functions and Mass Distributions

The anomalous gravity field is generated by variations in the density distribution inside the earth. Formally, we may write T as an integral over the earth

$$T = G \int_{\Omega} \frac{\Delta\rho}{r} \, d\Omega \tag{3.1}$$

where r is the distance, G the gravitation constant and $\Delta\rho$ the density <u>anomaly</u>, i.e.

$$\Delta\rho = \rho - \rho_0 \tag{3.2}$$

where ρ is the actual density and ρ_0 a normal density distribution, generating the normal potential. Opposed to ρ, $\Delta\rho$ may naturally attain both positive and negative values. When a reference field is utilized, the density anomalies may be viewed as being relative to a reference density distribution, generating the reference field. The reference distribution need usually not be given explicitly, it suffices simply to view it as the expected "normal" structure of the earth's interior. For more details, see e.g. Forsberg (1984).

In the sequel, the discussion of density distributions etc. should thus be understood in terms of density anomalies rather than just physical densities.

3.1 Deterministic Power Spectra of Elementary Masses

Power spectra of simple anomalous density bodies have widespread use in geophysical interpretation and also play a role in understanding the different types of covariance functions frequently used in geodesy. Consider first a <u>point mass</u>, or - equivalently - a sphere of constant density. The gravity effect in P for a sphere of mass m will be (cf. Figure 2)

$$g = Gm\frac{D}{r^3} \tag{3.1}$$

POINT MASS
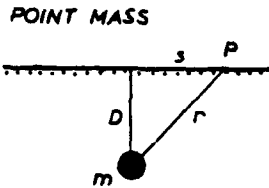
and thus by (2.23)

$$\tilde{g}(\omega) = 2\pi Gme^{-\omega D} \tag{3.2}$$

VERTICAL DIPOLE

For the gravity and potential power spectra thus

$$\phi_{gg}(\omega) = |\tilde{g}(\omega)|^2 = (2\pi Gm)^2 e^{-2\omega D} \sim e^{-2\omega D} \tag{3.3}$$

$$\phi_{TT}(\omega) = \frac{1}{\omega^2}\,\phi_{gg}(\omega) \sim \frac{1}{\omega^2}\,e^{-2\omega D} \tag{3.4}$$

VERTICAL MASS LINE
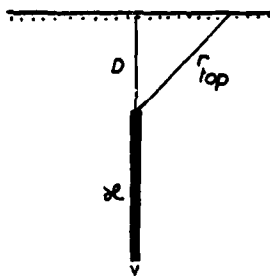
where "~" is used also for "proportional to".

For the <u>vertical dipole</u> of moment μ we have by well-known potential theory

$$T = G\mu\,\frac{D}{r^3} \tag{3.5}$$

Figure 2

and again for the spectrum

$$\tilde{T}(\omega) = 2\pi G\mu e^{-\omega D} \tag{3.6}$$

In this case the power spectra have more power at higher wave numbers:

$$\phi_{gg} \sim \omega^2 e^{-2\omega D} \tag{3.7}$$

$$\phi_{TT} \sim e^{-2\omega D} \tag{3.8}$$

The <u>vertical mass line</u> has less power at higher wave numbers. We have

$$g = G\kappa \int_{D}^{\infty} \frac{z}{r^3} dz = G\kappa \frac{1}{r_{top}} \tag{3.9}$$

where κ is the line mass density. Thus

$$\phi_{gg} \sim \frac{1}{\omega^2} e^{-2\omega D} \tag{3.10}$$

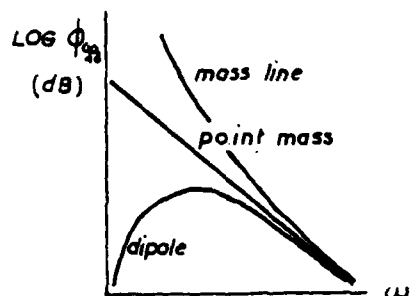$$\phi_{TT} \sim \frac{1}{\omega^4} e^{-2\omega D} \tag{3.11}$$

Figure 3

Conventionally in potential field analysis (gravity and magnetics), power spectra are plotted (single) logarithmic. In this case the point mass power spectrum will be a straight line, the slope of which is a direct measure of the depth D (Figure 3). This forms the base of spectral methods in geophysical inversion, especially used in magnetics. (In the magnetic case, gravity results may be transferred by using Poissons formula for the magnetic potential: $U = -\bar{m} \cdot \nabla T$, where $\bar{m}$ is the magnetization vector of the body in question. This implies e.g. that the gravity point mass spectrum corresponds to a magnetic vertical dipole line).

It is of interest also to consider the change in shape of the power spectra when the dimensions of the "anomalous body" are not negligible. To include "width" and "thickness" of the bod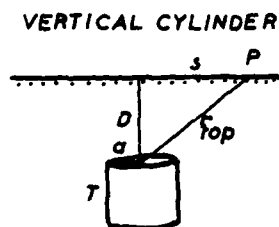y, consider a cylinder of constant density ρ, diameter 2a and thickness T (Figure 4). The gravity effect is one of the less trivial geophysical elementary bodies (the "volcanic plug"). Using (3.9) the attraction at P may be written

Figure 4

$$g(s) = G_0 \int_0^a (\frac{1}{r_t} - \frac{1}{r_b}) 2\pi a' da' \tag{3.12}$$

$$r_t^2 = (s - a')^2 + D^2, \qquad r_b^2 = (s - a')^2 + (D + T)^2$$

To get the spectrum, (3.12) is inserted into the Hankel transform integral (2.19):

$$\tilde{g}(\omega) = 2\pi \overline{g}(\omega) = 4\pi^2 G_0 \int_0^\infty \int_0^a (\frac{1}{r_t} - \frac{1}{r_b}) a' da' J_0(\omega s) s ds \tag{3.13}$$

which by interchange of integration order and some evaluations results in (Petersen, 1978)

$$\tilde{g}(\omega) = 2\pi Gm \cdot e^{-\omega D} \cdot \frac{1-e^{-\omega T}}{\omega T} \cdot \frac{J_1(a\omega)}{\frac{1}{2}a\omega}, \qquad m = \pi a^2 T \tag{3.14}$$

This is seen to be the point mass spectrum (3.2) multiplied by a thickness and a width factor (J_1 is the Bessel function of the order 1). These factors are shown in Figure 5 for unit radius and thickness. The factorization is typical for the spectra of "simple" bodies. A similar formula is obtained e.g. for the rectangular prism, see e.g. Forsberg (1984). Due to the factorization, the power spectrum becomes equally simple:
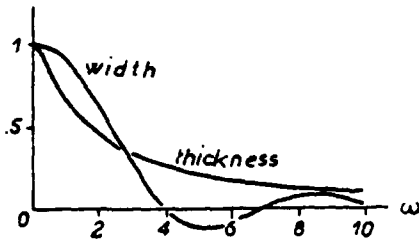
$$\phi_{gg}(\omega) \sim e^{-2\omega D} (\frac{1-e^{-\omega T}}{\omega T})^2 (\frac{J_1(a\omega)}{\frac{1}{2}a\omega})^2$$

Figure 5 When $T \ll D$ and $a \ll D$, the factors may be neglected, or, in other words, the point mass approximation is adequate.

3.2 Statistical Mass Distributions

The spectra of the "simple" bodies of the last section are encountered also when considering independent statistical <u>ensembles</u> of the same bodies. This is due to a fundamental theorem of statistical mechanics, stating that the mathematical

expectation of the "total" power spectrum equals the ensemble average of the "individual" power spectra.

Assume

$$\phi^P(\omega) = \phi^P(\omega, p_1, \ldots, p_k) \tag{3.16}$$

is the power spectrum of an individual body, characterized by parameters $p_1, \ldots, p_k$, describing e.g. depth, width, density etc. (radial symmetry has, for simplicity, been assumed). The distribution of the bodies is described by an ensemble joint frequency distribution $f(p_1, \ldots, p_k)$. Then the total power spectrum ϕ will be the ensemble average of ϕ^P:

$$\phi(\omega) = E\{\phi^P(\omega)\} = \int_{p_1} \cdots \int_{p_k} \phi^P(\omega, p_1, \ldots, p_k) \, f(p_1, \ldots, p_k) \, dp_1 \cdots dp_k \tag{3.17}$$

(Spector and Grant, 1970).

If the parameters are assumed to vary independently, then the joint frequency distribution will be a product $f(p_1, \ldots, p_k) = f_1(p_1) \ldots f_k(p_k)$. Of special interest is the case where the parameters are assumed to have a white noise distribution. In this case $\phi(\omega) = \phi^P(\omega)$, and we have immediately the following spectra for a "random" layer at depth D:

White noise density layer: $\qquad \phi_{gg}(\omega) \sim e^{-2\omega D}$ $\qquad\qquad$ (3.18)

White noise dipole layer: $\qquad \phi_{gg}(\omega) \sim \omega^2 e^{-2\omega D}$ $\qquad\qquad$ (3.19)

White noise "mass lines": $\qquad \phi_{gg}(\omega) \sim \frac{1}{\omega^2} e^{-2\omega D}$ $\qquad\qquad$ (3.20)

The white noise density layer may be interpreted physically as random undulations in the depth of the interface between two layers of constant density, e.g. a sediment/basement interface.
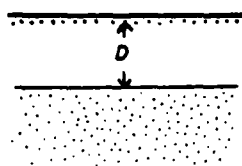
For an example with two parameters, consider an earth model of point masses of white-noise random mass and random depth below a layer at D (Figure 6). For this "all white" assemblage of mass points

Figure 6

$$\phi_{gg}(\omega) \sim \int_D^\infty e^{-2\omega D'} dD' \sim \frac{1}{\omega} e^{-2\omega D} \qquad (3.21)$$

and similarly for an "all-white" dipole distribution

$$\phi_{gg}(\omega) \sim \omega e^{-2\omega D} \qquad (3.22)$$

This may be generalized to the so-called <u>stationary thin layered earth model</u>, where the density anomaly distribution is assumed to be described by a covariance function and thus power spectrum $\phi_{\rho\rho}$. If the earth is assumed to consist of a number of thin layers (e.g. a sedimentary sequence), then each layer will yield a partial power spectrum of form

$$\phi_{gg}(\omega) = (2\pi G \Delta z)^2 \, \phi_{\rho\rho}(\omega, \, d) e^{-2\omega d} \qquad (3.23)$$

where d is the depth and Δz the thickness.

If the layers are similar and independent, the total power spectrum thus will be

$$\phi_{gg}(\omega) \sim \phi_{\rho\rho}(\omega) \, \frac{1}{\omega} \, e^{-2\omega D} \qquad (3.24)$$

yielding an example of a one-to-one relationship between gravity and density co-variance functions.

The above examples all have in common the factor $e^{-2\omega D}$, containing the depth information. This factor is the prime "objective" of the widespread statistical inversion techniques of geophysical inversion applied successfully for more than a decade, especially for aeromagnetic data. In the method, depths to the top

and base of magnetized layers may be found (at times also width parameters are solved for), using the shape of the power spectrum, computed for a given area. Layers at various depth's typically show up as more or less straight line segments in the power spectrum, when plotted logarithmic, and depths are derived from the slope values. Examples may be found e.g. in Spector and Grant (1970).

An impressive example of a two-layer magnetic problem may be seen in the global degree variances of the magnetic field (Figure 7). The field from the earth's core is seen to dominate up to $\ell \dot{=} 13$, after which the "shallow" crustal field takes over. The core radius inferred from the slope of the low degree variances, yields a value only a few hundred kilometers deeper than the seismically determined value (3485 km).
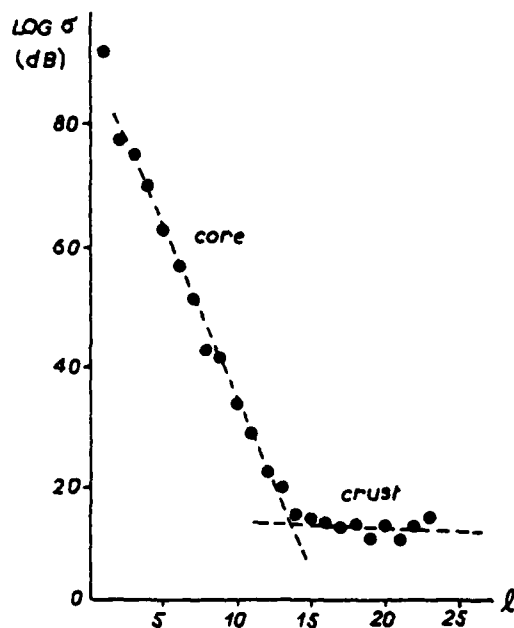
Figure 7 Degree-variances for the earth's magnetic field. MAGSAT solution, complete to degree and order 23 (after Langel)

While the statistical approaches have proved very successful for magnetic data, they have been less applicable to gravity interpretation. This is partly due to the (usually) less dense gravity coverage, and, especially, to the different nature of the sources: density anomaly variations tend to be more "spread out" and less random than changes in magnetization and susceptibility. The

typical "clear-cut" geophysical problem of unmagnetic sediments overlying a highly magnetized methamorphic basement has e.g. usually a much less clear gravity parallel, intra-sedimentary density anomalies being most often non-negligible.

However, the value of the statistical interpretation for gravity is yet high: it provides an efficient means for a deeper understanding of covariance functions, as outlined in the sequel.

3.3. Relationship to Traditional Covariance Functions

Most frequently simple, analytical covariance functions have been used for e.g. gravity field modelling by collocation. These functions are characterized by a few "free" parameters, which may be adjusted to fit the "essential" parameters of a local covariance function, such as (gravity) variance C_0, correlation length $x_{\frac{1}{2}}$ and horizontal gravity gradient variance G_0, for a discussion see Moritz (1980, ch. 22).

For the planar case many different types of analytical covariance functions have been suggested: e.g. exponential, Gaussian and especially models of form

$$C(s) = \frac{C_0}{(1+(s/D')^2)^m} \qquad (3.25)$$

where D' and m are constants. However, of these simple models, only two allow the derived <u>spatial</u> covariances $C(s, z_1, z_2)$ to have correspondingly simple expressions: namely (3.25) for $m=1/2$ and $m=3/2$, see again Moritz (1980). The covariance functions

$$C(s) = \frac{C_0}{(1+(\frac{s}{D'})^2)^{\frac{1}{2}}} \qquad (3.26)$$

and

$$C(s) = \frac{C_0}{(1+(\frac{s}{D'})^2)^{\frac{3}{2}}} \qquad (3.27)$$

have been termed the <u>reciprocal distance</u> and the <u>Poisson</u> covariance functions respectively. The associated power spectra follow from (2.22) and (2.23):

Reciprocal distance: $\qquad \phi_{gg} = 2\pi C_0 D' \frac{1}{\omega} e^{-\omega D'}$ $\qquad$ (3.28)

Poisson: $\qquad \phi_{gg} = 2\pi C_0 D'^2 e^{-\omega D'}$ $\qquad$ (3.29)

Thus, by (3.22) the reciprocal distance covariance function may be interpreted as generated by an "all-white" assemblage of mass points from depth $D=\frac{1}{2}D'$, or in other words - a stationary, thin-layered earth with a white noise density anomaly distribution below depth D. The Poisson covariance function may similarly be interpreted as associated with a white noise density layer at depth $D=\frac{1}{2}D'$.

For spherical covariance models a number of expressions have been used or suggested. Generally, the covariance models have been obtained from selected models of the degree-variances, where the spatial covariances may be evaluated by analytical expressions.

At sea level the general expression for the potential covariance function may be written

$$K(\psi) = \sum_{\ell=2}^{\infty} \sigma_\ell \left(\frac{R_b^2}{R^2}\right)^{\ell+1} P_\ell(\cos \psi) \qquad (3.30)$$

where R_b is the radius of the Bjerhammar sphere and $R > R_b$ an earth radius. The depth to the Bjerhammar sphere is directly related to the depth parameter D of the planar covariance functions: When $R-R_b \ll R$ then

$$\left(\frac{R_b^2}{R^2}\right)^{\ell+1} = \exp(2(\ell+1) \log(\frac{R_b}{R})) \approx e^{-2\omega D}, \qquad \omega = \frac{\ell+1}{R}, \qquad D = R-R_b \qquad (3.31)$$

Thus for large ℓ, the asymptotic degree variances for the reciprocal distance and Poisson covariance functions must be of the form

Reciprocal distance: $\qquad \sigma_\ell \sim \frac{1}{\ell^2} \sigma^{\ell+1} \quad (\sigma = \frac{R_b^2}{R^2})$ $\qquad$ (3.32)

Poisson: $\qquad \sigma_\ell \sim \frac{1}{\ell} \sigma^{\ell+1}$ $\qquad$ (3.33)

This follows directly from the relationship (2.34) between the power spectrum
and the degree variances. Closed formulas for the spherical reciprocal distance
and Poisson covariance functions are found in Moritz (1980, ch. 23).

An important additional class of degree-variance models is the

$$\text{Logarithmic:} \quad \sigma_\ell \sim \frac{1}{\ell^3} \sigma^{\ell+1} \tag{3.34}$$

The earth's gravity field is known to adhere to such a power law on a global scale.
Well known empirical logarithmic models are "Kaula's Rule"

$$\sigma_\ell \approx 0.7 \cdot 10^{-10} \frac{2\ell+1}{\ell^4} \tag{3.35}$$

(see e.g. Phillips and Lambeck, 1980) and the "Tscherning-Rapp" model

$$\sigma_\ell = 4.4 \cdot 10^{-10} \cdot \frac{1}{(\ell-1)(\ell-2)(\ell+24)} \cdot .99962^{\ell+1} \tag{3.36}$$

(Tscherning and Rapp, 1974), which corresponds to a Bjerhammar sphere depth of
1.2 km. From (3.34) follows that the asymptotic form of the logarithmic power
spectrum is

$$\phi_{gg}(\omega) \sim \frac{1}{\omega^2} e^{-2\omega D} \tag{3.37}$$

which is seen to be the "white mass lines" power spectrum. A more reasonable
physical model is obtained by the stationary, thin-earth assumption: then from
(3.24) the density spectrum must be of the form

$$\phi_{\rho\rho}(\omega) \sim \frac{1}{\omega} \tag{3.38}$$

which is a plausible "red noise" spectrum with high power in the low wave numbers.
However, such a noise model globally implies stresses in the interior of the earth
that are bigger than the stress which e.g. the mantle is currently thought to

be able to sustain: therefore "multilayer" models are more adequate for obtaining realistic statistical density models. Naturally such models in addition may provide a better fit to empirical data, since more free parameters will be available to "tune" the covariance model.

Heller's <u>attenuated white noise (AWN) model</u> is an example of this kind. In the AWN model the global degree-variances are modelled using 5 density shells at various depths, where the potential originating from each shell is assumed to be white noise at the shelf itself, i.e.

$$\sigma_\ell \sim \sum_{i=1}^{5} a_i(2\ell+1)(\frac{(R-D_i)^2}{R^2})^{\ell+1} \tag{3.39}$$

where a_i and D_i are constants (Jordan, 1978). For each shell, the associated planar power spectrum will be of form

$$\phi_{gg} \sim \omega^2 e^{-2\omega D_i} \tag{3.40}$$

and thus the AWN-model may be interpreted as a <u>white noise dipole layer</u> model.

The various simple covariance models are listed in Table 1, showing the unnormalized <u>forms</u> of the gravity power spectrum $\phi_{gg}(\omega)$, covariance function $C(s)$ and degree-variances σ_ℓ using (2.34)

Table 1

Density Model	$\phi_{gg}(\omega)$	$C(s)$	Asymtotic σ_ℓ	Covariance type (Moritz)
white mass lines	$\frac{1}{\omega^2} e^{-2\omega D}$	$-\log(D'+r)$	$\frac{1}{\ell^3}$	"logarithmic"
"all-white" masses	$\frac{1}{\omega} e^{-2\omega D}$	$\frac{1}{r}$	$\frac{1}{\ell^2}$	"reciprocal distance"
white mass layer	$e^{-2\omega D}$	$\frac{D'}{r^3}$	$\frac{1}{\ell}$	"Poisson"
"all-white" dipoles	$\omega e^{-2\omega D}$	$\frac{3D'^2}{r^5} - \frac{1}{r^3}$	const.	
white dipole layer	$\omega^2 e^{-2\omega D}$	$\frac{15D'^3}{r^7} - \frac{3D'}{r^5}$	ℓ	"AWN"

Note: $D' = 2D$, $r = \sqrt{D'^2+s^2}$

The covariance function expressions have been given by (3.26) and (3.27) for the "reciprocal distance" and "Poisson", respectively. The remaining covariance functions have been derived utilizing the relationships

$$\omega \cdot \phi_{gg} \longleftrightarrow \text{differentiation } \frac{d}{dD'}$$

$$\phi_{gg}/\omega \longleftrightarrow \text{integration after } D'$$

between frequency domain and space domain. Thus, C(s) one step downwards in the table is obtained by differentiation, C(s) one step upwards is obtained by integration.

Correspondingly, since for the potential power spectrum

$$\phi_{TT}(\omega) = \frac{1}{\omega^2} \phi_{gg}(\omega) \tag{3.41}$$

the form of the <u>potential</u> covariance function K(s) may be found going <u>two steps up</u> in the table, and similarly second-order gradient covariances may be found going two steps <u>down</u>.

When going "upwards" in the table, the covariance function C is seen to be less and less "sharp", and from the "logarithmic" level (and upwards) it will be <u>singular</u>, going to minus infinity for large r. This singularity is a consequence of the inadequacy of the planar approximation for low wave numbers . The large power at low wave numbers ($\frac{1}{\omega^2}$ in the "logarithmic" case) will not be found on <u>actual</u> power spectra, since the use of a spherical harmonic reference field will remove the power at the lowest wave numbers. For all the simple power spectra of Table 1, such suppression of low wave numbers will result in well-behaved covariance functions C. In principle, the necessary suppression of low wave numbers is corresponding to the omission of the lowest degree-variances (e.g. $\ell=0$ and 1) in the spherical covariance expression.

The suppression of the low wave numbers will be treated in more detail later in this report. First, however, attention will be given to the covariance expressions C(s). Their simple forms allow a straightforward interpretation of collocation in terms of "generalized point mass" modelling under certain conditions.

4. Collocation as Generalized Point Mass Modelling

4.1 Covariances as Gravimetric Effects

The covariance expression C(s) of Table 1 may be viewed as <u>gravity effects</u> for points at the reference level. An example: consider two points P and Q with distance S. Then the gravity covariance C(P, Q) for a white noise density layer at depth D (the Poisson covariance) corresponds to the gravity effect in Q from a point mass at depth 2D below P:
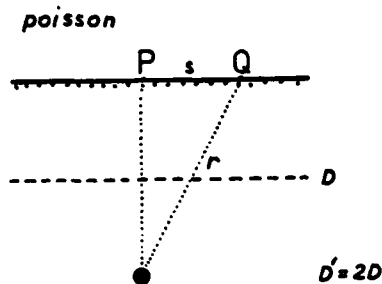
$$\text{"Poisson"} \quad C(P,\ Q) \sim \Delta g^P(Q)$$

cf. Figure 8.
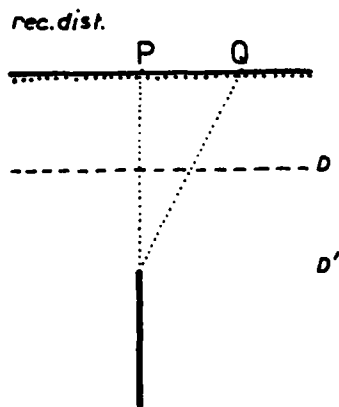
Similarly the "reciprocal distance" covariance function ("all white" masses) corresponds to the mass line effect, while the logarithmic covariance may be viewed as generated by a rather strange mass body: a "wedge", i.e. a mass line distribution with line mass density κ increasing linearly downwards (Figure 8).

Thus, the "successive" covariance functions of Table 1 are generated by the following "generalized point masses":
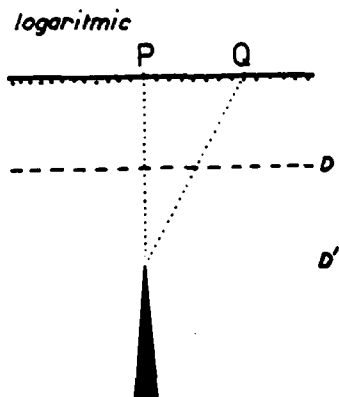
|		
"logarithmic"	:	mass wedge
"rec. dist."	:	mass line
"Poisson"	:	point mass
---	:	dipole
AWN	:	quadropole

(these "deterministic" mass distributions should, of course, not be mixed with the statistical density models of the previous section).

poisson

rec.dist.

logaritmic

Figure 8

In fact, _any_ covariance function C(s) may be interpreted as some line mass effect:

Assume C to be the gravity effect of a mass line below P of line density $\kappa(t)$, where $t=-z$ is the depth coordinate (Figure 9). Now,

$$C(s) = G \int_0^\infty \frac{\kappa(t)}{r^3} t\, dt \qquad (r = \sqrt{s^2+t^2}) \qquad (4.1)$$
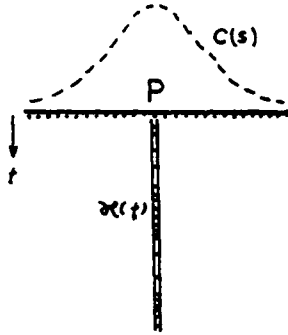
Figure 9

and by taking the Fourier transform and interchanging the order of integration

$$\phi_{gg}(\omega) = 2\pi G \int_0^\infty \kappa(t)\, e^{-\omega t} dt \qquad (4.2)$$

Again (2.3) has been used. Thus, the power spectrum ϕ_{gg} is given as the Laplace transform of κ. Conversely, given C, κ may be found by an inverse Laplace transform of the associated power spectrum. Due to the properties of the Laplace transform, the transition $C \longleftrightarrow \kappa$ is in principle unique and exists for all reasonable covariance functions.

The gravimetric interpretation also holds for covariances aloft under certain conditions. If P is at reference level, but Q at altitude z, then by (2.27):

$$C(P, Q) = \frac{1}{2\pi} \int_0^\infty \omega \phi_{gg}(\omega)\, e^{-\omega z} J_0(s\omega) d\omega \qquad (4.3)$$

By inserting (4.2) and interchanging the order of integration then

$$C(P, Q) = G \int_0^\infty \kappa(t) \int_0^\infty \omega e^{-\omega(t+z)} J_0(s\omega) d\omega dt \qquad (4.4)$$

$$= G \int_0^\infty \frac{\kappa(t)}{[s^2+(t+z)^2]^{3/2}} (t+z) dt \qquad (4.5)$$

which is simply the gravity effect at Q. If both P and Q are at altitude, then z in (4.5) should be replaced by z_P+z_Q. The "gravity interpretation" of a covariance function C(s) thus allows an easy extension to the spatial covariance $C(s, z_P, z_Q)$.

4.2 Application to Least Squares Collocation

In the statistical formulation of least squares collocation a signal s is estimated from a vector of measurements x, the estimate being given by the well-known formula

$$\hat{s} = C_{sx} C_{xx}^{-1} x \tag{4.6}$$

The cross- and auto-covariances C_{sx} and C_{xx} are obtained by covariance propogation

$$\{C_{sx}\}_i = L_s L_{P_i} K(\cdot, \cdot) \tag{4.7}$$

$$\{C_{xx}\}_{ij} = L_{P_i} L_{P_j} K(\cdot, \cdot) \tag{4.8}$$

where the signal $s = L_s(T)$ and observations $x_i = L_{P_i}(T)$ are viewed as linear functionals (the dots in (4.7) and (4.8) indicate that the functionals should be applied on separate variables of the potential covariance function $K(P, Q)$).

For practical solutions, $\hat{s}$ is obtained as a linear combination

$$\hat{s} = \sum_i a_i \{C_{sx}\}_i \tag{4.9}$$

with coefficients a_i given as the solution to the "normal equations"

$$\sum_i \{C_{xx}\}_{ij} a_i = x_j \tag{4.10}$$

Consider now the simple case of the observations being <u>gravity anomalies</u> at a set of points P_i, and assume the <u>Poisson covariance function</u> to be used. Then, with the interpretation of covariances in terms of gravity effects, the covariances may, as earlier mentioned, be written as

$$\{C_{xx}\}_{ij} = \Delta g^i(P_j) \tag{4.11}$$

where Δg^i represents the gravity effect of a mass point of unit mass, located below P_i at a depth D' determined by the chosen correlation length $x_{\frac{1}{2}}$ of the Poisson covariance function used, i.e. $D' \cong 1.30 \, x_{\frac{1}{2}}$, as may easily be verified.

Then (4.10) may be written as

$$\sum_i \Delta g^i(P_j) \, a_i = x_j \qquad (4.12)$$

which is nothing but the inversion equation of point mass modelling, with point masses located below all points P_j. Thus collocation and point mass modelling are <u>identical</u> when the Poisson covariance function is used, and signal estimates (4.9) are simply obtained as the relevant computed gravity field quantity from the point masses, the mass point below the i'th gravity point having mass a_i.

For other types of covariance functions, collocation may similarly be viewed as generalized point mass modelling, where point masses are then replaced by the other "elementary" mass bodies (cf. Section 4.1). In e.g. the AWN case, collocation thus corresponds to solving for a number of quadropole moments while e.g. the logarithmic covariance functions correspond to "mass wedge" modelling.

The above only hold when exclusively gravity data are used as observations. For <u>heterogenous</u> data, e.g. a mixture of gravity and geoid observations, the simple scheme must be modified so that the type of elementary mass model to be used below an observation point will be dependent on the type of gravity field data given at the point.
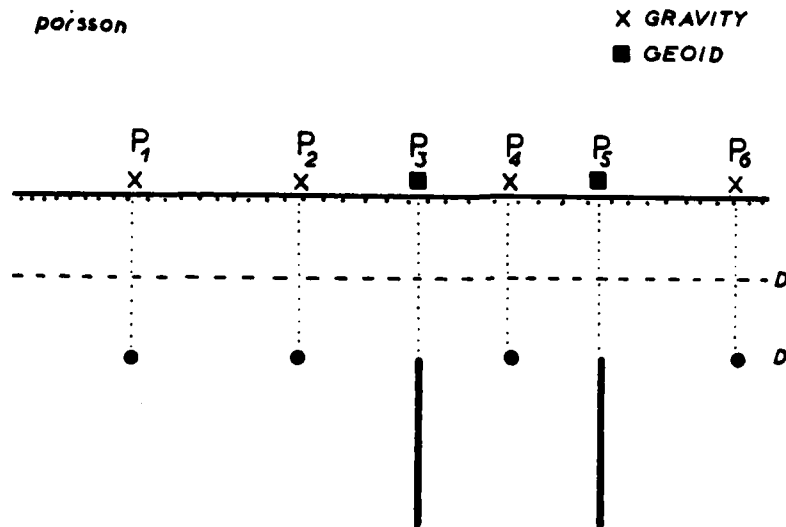
Consider again the Poisson covariance function, and assume a mixture of gravity and geoid data to be given at the reference plane, e.g. representing available gravity field data in an oceanic area. Then the covariances in C_{xx} between gravity stations are identical to point mass effects. Between points with geoid observations, the covariances will be (essentially) $K(\psi)$, which will be of form $-\log(D'+r)$, cf. Table 1, which is the form of the geoid effect of the vertical mass line with top at depth D'. Similarly, geoid-gravity cross covariances may be interpreted as the gravity effect of the vertical mass line, or - equivalently - the geoid effect of the point mass.

In this case thus (4.10) may again be viewed as an inversion equation, where the unknowns to be solved for will be for

Gravity stations: point mass values

Geoid points   : line density values

as shown schematically in Figure 10. Other gravity field data types have similar associated "inversion masses": second-order gradients, e.g. T_{zz}, corresponds to a dipole point, while deflections of the vertical like gravity corresponds to the point mass.

Figure 10 Collocation as generalized point mass modelling. With the Poisson covariance function ("white noise density at depth D"), collocation corresponds to solving for point masses and line mass densities at depth D'=2D, satisfying the given observation data.

The view of collocation as a generalized point mass modelling technique is of course primarily of interest as a tool for a better clarification of what is "going on" when using least squares collocation. Naturally, the practical work remains the same, namely to solve a system of linear equations containing one equation for each observation point and predict "signals" by summing up the solution coefficients times the relevant cross-covariances.

While collocation in general may be viewed as generalized point mass modeling, traditional mass modelling approaches are not necessarily corresponding to collocation. Only when the number of unknowns equals the number of observations (and each "mass point" is situated immediately below an observation point) will the result of point mass modelling be a collocation solution: point mass modelling of gravity data corresponds to the use of Poisson's covariance function, dipole

modelling to the "all-white dipoles" covariance function (one step down in Table 1)
etc. Since the earth's actual gravity field variations tend to be best described
by *logarithmic* covariance functions, "optimum" results should thus be obtained
with some "mass wedge" type inversion.

5. Application of Simple Covariance Models for Local Covariance Functions

After the "side jump" of the last section to collocation, emphasis will now
return to the statistical density distributions and the associated covariance
functions.

5.1 Use of Multi-Layer Models

The simple covariance functions of the previous sections may be used to build
good approximations to empirical covariance functions through the use of multi-
layer models.

Consider the simple case of a number of white noise density layers, representing
e.g. interfaces at a layered earth model. If the undulations of the interfaces
are assumed statistically independent (like the *"thin-layered stationary earth
models"*), then the total covariance function will be the sum of the individual
(Poisson) covariance functions

$$C(s) = \sum_i C_i(s) \sim \sum_i \frac{m_i}{\Sigma m_i} \frac{2D_i}{r_i^3} , \quad r_i = \sqrt{s^2 + (2D_i)^2} \quad (5.1)$$

as illustrated in Figure 11 (m_i is the variance of each mass plane density dis-
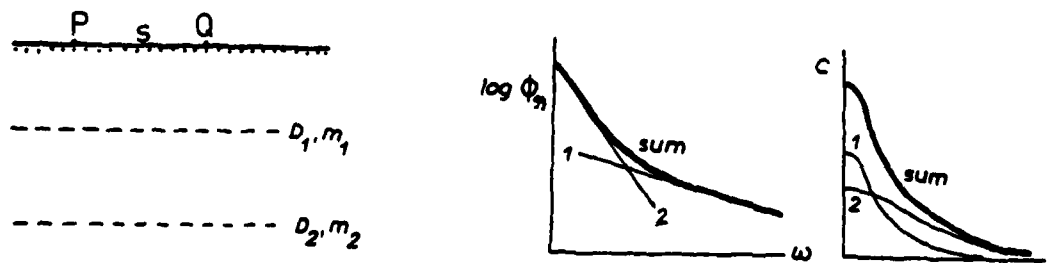tribution).

Figure 11 Two-layer stationary density model with associated power spectrum and
covariance function.

By adjusting the "free" parameters (D_i, m_i) good approximations to empirical co-
variance funcations may be obtained.[*]

The depth and density parameters may be chosen based on geological considera-
tions or - usually more realistic - based on the shape of the computed empirical
power spectra. If the gravity field sources at a certain depth range tend to
behave like a white noise layer, then the power spectrum tend to show straight-
line segments at a wavelength band corresponding to the depth range, when plotted
logarithmic.

An actual data example (Ohio area) is shown in Figure 12. In this example
a reasonably good covariance fit is obtained using a two layer model, with depths
determined from the shape of the two fitted lines. Below 0.5 cycle/degree, cor-
responding to spherical harmonic degree 180, the model should not fit, since har-
monics below 180 have been attempted to be removed by utilization of a 180 x 180
reference field (the apparent existence of power below 0.5 cycle/degree is due
to errors in this reference field).

In the Ohio example, the two depth values represent the average influence
of shallow and deep sources. Considering the geology (primarily a paleozoic sedi-
mentary basin of thickness of order-of-magnitude D_1), the two covariance model
constituents may be ascribed as originating primarily from sedimentary sources
and deep crustal sources, (e.g. undulations of the "conrad" discontinuity) respec-
tively. Such an interpretation should, however, be taken with great caution.
The area is so big that there is no reason to expect the geology to be so "constant"
that the layering of the crust "shines through" to the estimated power spectrum,
and also the shallow depth parameter is affected by important error sources such
as data noise and aliasing.

With the two-component description of the power spectrum, it is easy, by
simple graphical techniques, to subdivide the gravity field variation into two
parts, representing each source.

Each component is a Poisson covariance function of the form

$$C(s) = C_0 \frac{D'^3}{[s^2+D'^2]^{3/2}} \qquad (D'=2D) \qquad (5.2)$$

[*] Note that with e.g. simple Poisson covariance functions, C(s) can never be negative.
However, for practical applications the covariance functions need to be modified
by removing power at the lowest wave numbers, to avoid the singularities in the
elementary functions caused by the deficiency of the planar approximation for low
wave numbers. After this "removal" negative covariances may be obtained as well.
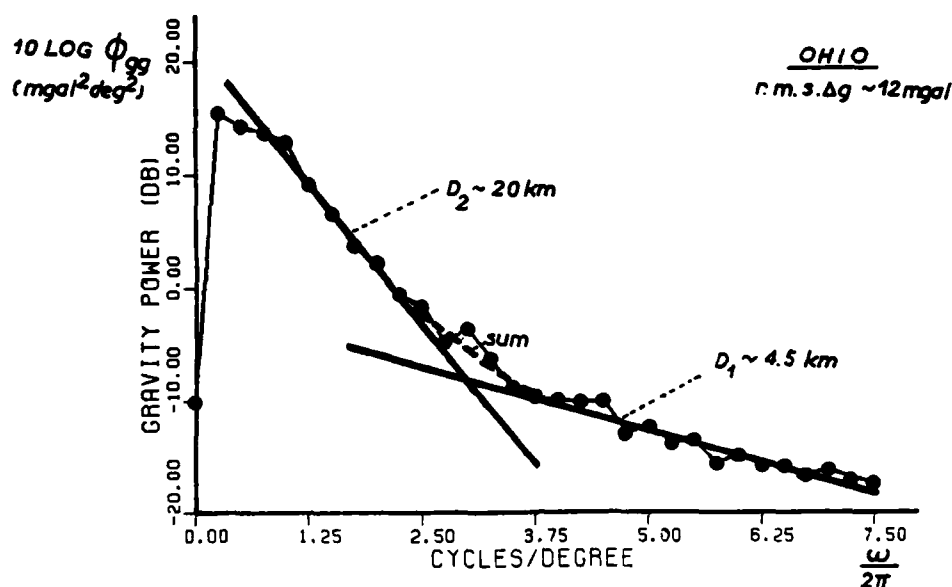More details in the next section.

Figure 12   Empirical power spectrum for residual free-air anomalies with respect
to Rapp's 180 x 180 spherical harmonic expansion.   Area bounded by
latitude 38°-42° N and longitude 85° to 81° W.   Data points (shown
with dots) obtained from 4'x 4' gridded gravity data using a 2-dimen-
sional FFT and radial smoothing.

which as earlier mentioned has the power spectrum

$$\phi_{gg}(\omega) = 2\pi C_0 D'^2 e^{-\omega D'} \tag{5.3}$$

Looking at Figure 12, the ratio between the two components at DC ($\omega=0$) is seen
to be around 23 dB which by (5.3) results in a gravity variance ratio of 0.099 between
the shallow and deep components, respectively.   From the total gravity variance
(153 mgal²) the r.m.s. variation of the shallow and deep components then becomes
3.7 and 11.8 mgal respectively.

5.2 Modifications to Eliminate the Influence of Low Frequencies

If one tried to estimate geoid variances for the Ohio example, one would
find that the derived variances turned out to be infinite.[*]   What is wrong is
that the "elementary" Poisson covariance function contains too much power at the
lowest frequencies near DC, where the planar approximation is not valid.

---

[*]The associated potential covariance function K(s) will be of form -log(D'+r),
cf. Table 1.

This is not the case for all of the covariance models of Table 1. For instance the AWN model has well-behaved geoid variances even in the planar case. On the other hand, however, the logarithmic covariance function is even for gravity anomalies singular, since the derived covariance function C(s) does not go to zero for large s, cf. Table 1.

There is therefore a need for modification of the simple covariance models, so that the power at the low frequencies is suppressed. This is necessary not only due to the singularities induced by the flat-earth approximation - it is always needed for local covariance functions when a spherical harmonic reference field has been removed, irrespectively of whether a flat-earth or a round-earth formulation is used.

If the spherical harmonic reference field was assumed to be error-free, the natural modification would be to truncate the "elementary" power spectra like (5.3) below the wave number corresponding to the maximal degree of the spherical harmonic expansion. The covariance function C(s) is then derived by Hankel transformation of the truncated power spectrum, e.g. for a Poisson covariance

$$
\phi_{gg}^{t}(\omega) = \begin{cases} 0 & \omega \leq \omega_t \\ 2\pi C_0 D'^2 e^{-\omega D'} & \omega > \omega_t \end{cases}
\tag{5.4}
$$

where the truncation wave number for a reference field complete to spherical harmonic degree ℓ_{max} should be $\omega_t = \frac{\ell_{max}}{R}$.

With this approach there are drawbacks: First, no simple analytical expressions exist for the covariance functions, necessitating the use of e.g. numerical integration techniques, and secondly for practical applications some energy should be left below ω_t, to take into account errors in the spherical harmonic reference field (these errors are believed to be of the same order of magnitude as the degree-variances themselves for the higher degrees in existing 180×180 solutions, see e.g. Rapp, 1981).

Figure 13
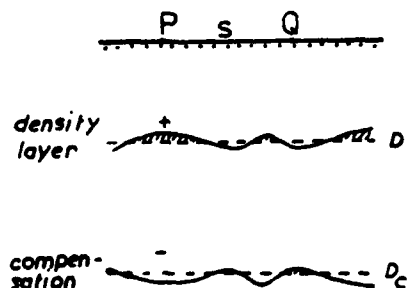
Relatively simple analytical expressions may be obtained by an approximative alternative approach based on a pseudo-isostatic formulation. Assume the density anomalies to be described by a white-noise layer model at depth D, and assume that this layer is perfectly isostatically compensated at a deeper level D_c. The power spectrum of this "compensated Poisson model" will be of form

$$\phi_{gg}(\omega) = 2\pi\alpha(e^{-\omega D} - e^{-\omega D_c})^2 \tag{5.5}$$

where α is a constant. The formula follows simply from (3.2), since the spectrum due to the ensemble averaging theorem will have the same form as the spectrum of a positive/negative mass point pair. The spectrum (5.5) will be a linear combination of three simple poisson spectra of depths D, D_c and $D_m = \frac{1}{2}(D+D_c)$:

$$\phi_{gg}(\omega) = 2\pi\alpha(e^{-2\omega D} + e^{-2\omega D_c} - 2e^{-2\omega D_m}) \tag{5.6}$$

The power spectrum may adequately be written

$$\phi_{gg}(\omega) = 2\pi\alpha e^{-2\omega D}(1 - e^{-\omega T})^2, \qquad T = D - D_c \tag{5.7}$$

to show more directly how the introduction of the compensating layer corresponds to suppression of power at low wave numbers (Figure 14).
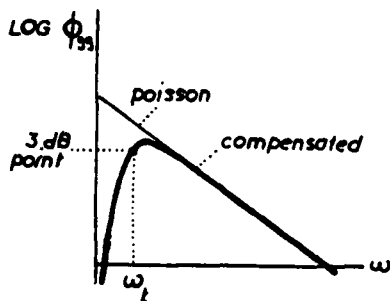

The choice of compensation depth will be dependent on ℓ_{max} for the spherical harmonic reference expansion. For e.g. a 180×180 field, ω_t may arbitrarily be put at the point where the "compensated" power has dropped 3dB (i.e. half) below the simple Poisson expression, i.e.

Figure 14

$$e^{-2\omega_t D}(1 - e^{-\omega_t T})^2 = 0.5\, e^{-2\omega_t D}, \qquad \omega_t = \frac{\ell_{max}}{R} \tag{5.8}$$

giving T=43 km. Thus, the use of commonly accepted "realistic" isostatic parameters corresponds quite closely to spherical harmonic reference fields with ℓ_{max} around 180.

The covariance function for the compensated model will like (5.6) be a linear combination of simple Poisson covariance functions

$$C(s) = \alpha(\frac{D'}{r^3} + \frac{D'_c}{r_c^3} - 2\frac{D'_m}{r_m^3}) \;, \quad D'=2D, \; D'_c=2D_c, \; D'_m=D+D_c,$$

$$r = \sqrt{s^2+D'^2} \; \text{etc.} \tag{5.9}$$

The potential covariance function $K(s)$ corresponding to (5.9) will be (cf. Table 1)

$$K(s) = \alpha(-\log(D'+r) - \log(D'_c+r_c) + 2\log(D'_m+r_m))$$

$$= \alpha \; \log \frac{(D'_m+r_m)^2}{(D'+r)(D'_c+r)} \tag{5.10}$$

which does not exhibit the singularities of the individual "components", the geoid variance being

$$\sigma_n^2 = \frac{1}{\gamma^2} \; K(0) = \frac{\alpha}{\gamma^2} \; \log \frac{D_m^2}{D \; D_c} \tag{5.11}$$

The depths D and D_c are assumed to have been chosen e.g. based on a power spectrum analysis. The constant α are then given from the gravity variance $C(0) = \sigma_{\Delta g}^2$ as

$$C(0) = \alpha(\frac{1}{D'^2} + \frac{1}{D_c'^2} - \frac{2}{D_m'^2}) \tag{5.12}$$

which by introduction of a dimensionless "variance scaling factor" β yields

$$\alpha = 4D^2 C(0)\beta, \qquad \beta = \frac{1}{1 + \frac{D^2}{D_c^2} - 2\frac{D^2}{D_m^2}} \tag{5.13}$$

The factor β takes into account the "lost" power at low frequencies compared to the simple Poisson model.

Returning to the Ohio example (Figure 12), estimates for the geoid undulations associated with the two source components may now be found. By inspecting Figure 12, a fairly large amount of power is seen to remain below 0.5 cycles/degree, corresponding to $\ell=180$. Therefore, to take into account also errors of the reference model, a fairly deep compensation level D_c is needed. From the position of the 3 dB-point a value of around 100 km seems to be reasonable.

For $D_c=100$ km, the β-factors for the 4.5 km and 20 km-layers are 1.01 and 1.22 respectively. Therefore the 23 dB difference on the DC-values corresponds to the slightly different variance ratio of 0.120, yielding r.m.s. variations for the shallow and deep components at 4.0 mgal and 11.7 mgal. Using these numbers and (5.11) and (5.13) the r.m.s. geoid variations are then found to be 5.0 cm and 40.5 cm, yielding a total r.m.s. geoid variation of 40.8 cm. The use of a more shallow compensation level means that the variance estimates contain less of the errors of the reference field. For $D_c=50$ km, the r.m.s. geoid variations thus diminish to 5.0 cm and 29.5 cm for the shallow and deep sources, corresponding to a total variation of 29.9 cm. For a crude comparison it may be mentioned that 9 GPS-determined geoid undulations in a smaller area of central Ohio (area extent ~ max. 40 km) have yielded a standard deviation of the 9 points around 22 cm (number derived from undulation difference data given by Engelis et al., 1984.)

To complete the discussion of the "compensated" model, finally second order derivatives will be considered. Since these quantities primarily are due to shallow, high-frequency gravity field variations, little difference would be expected between the "simple" and "compensated" Poisson model. In fact, it turns out that the scaling factor β exactly opposes the compensation effect, yielding identical variance expressions in the two cases.

Consider first the vertical gravity gradient. The "Poisson" covariance function of this quantity will be

$$G'(s) = C_0 D'^2 \left(\frac{15D'^3}{r^7} - \frac{3D'}{r^5}\right) \tag{5.14}$$

(cf. Table 1), and thus the familiar horizontal gradient variance G_0 (Moritz 1980, p. 177) is seen to be

$$G_0 = \frac{1}{2}G'(0) = \frac{6C_0}{D'^2} = \frac{3}{2}\frac{C_0}{D^2} \tag{5.15}$$

For the compensated model, variance scaling yields similarly by (5.13)

$$G_0 = \frac{3}{2} \beta C_0 \left(\frac{1}{D^2} + \frac{1}{D_c^2} - \frac{2}{D_m^2} \right) = \frac{3}{2} \frac{C_0}{D^2} \qquad (5.16)$$

i.e. an identical expression.

In the Ohio example, the shallow and deep sources thus correspond to r.m.s. gradient variations ($\sqrt{G_0}$) of 10.9 E and 7.1 E respectively (1 E=10^{-4}mgal/m), with a total r.m.s. variation of 13.0 E. This number may again be compared with observation data. Ca. 300 torsion balance stations exist in an area of south-western Ohio (surveyed by Badekas of O.S.U. nearly two decades ago), and for these stations a $\sqrt{G_0}$-value of c. 18 E was found (Tscherning, 1976, Figure 2a). The variances compare reasonably well, especially considering the limited resolution of the gravity data (4' grid) underlying the power spectrum plot of Figure 12.

The combined results of the Ohio example used in this section are shown in Table 2. Deflections of the vertical follow simply from the gravity results using the conversion factor 6.7 mgal/arcsec of section 2.1. A more thorough 3-layer analysis of part of this example area will be included in the next section.

Table 2

Two-Component Covariance Model for Ohio 4°x 4° area.
(white noise compensated density layer representation, Rapp-180 reference field)

Source	Depth (km)	C(0) (mgal²)	r.m.s. variation of			
			geoid (m)	deflections (arcsec)	free-air gravity (mgal)	gravity gradient (E)
"sedimentary"	4.5	16.3	0.05	0.6	4.0	10.9
"deep crustal"	20	136.7	0.40	1.7	11.7	7.1
total	--	153.0	0.41	1.8	12.4	13.0

6. Examples of Local Empirical Covariance Functions and Power Spectra

In this section some examples will be given on the shape of local power spectra and covariance functions for gravity anomalies in selected areas of the United States. Areas of fairly dense anomaly coverage have been chosen, in order to get the best estimates of the power spectra so that possible "straight-line segments" associated with major geologic interfaces would show up more clearly. Also, areas of dense data coverage permits the degree-variances to be derived with confidence up to high degrees, in the present study to $\ell=5400$.

The data used - free-air anomalies and terrain-corrected Bouguer anomalies - were supplied by the National Geodetic Survey. In order to work with local co-variance functions, the "Rapp-180" spherical harmonic expansion of the geopotential, complete to degree and order 180 (Rapp, 1981), has been subtracted for all data to yield residual anomalies. Furthermore, since one of the primary interests is in possible "geologic" effects in the power spectrum, the influence of the topography has been removed in the mountainous areas. The elimination of the topographic effects on the gravity anomalies has been done using a residual terrain model (RTM) reduction, where topographic irregularities relative to a smooth mean elevation surface are computationally removed. As mean elevation surface a spherical harmonic expansion of the topography, corresponding to the gravity expansion, has been used (Rapp, 1982).

The RTM-reduction is very convenient, since it effectively corresponds to a removal of all topographic effects above $\ell=180$, while nothing in principle is done below this degree (the "Rapp-180" gravity field also contains effects of the topography). As shown in (Forsberg, 1984), the RTM reduction corresponds usually within a fraction of a mgal to a Bouguer reduction to the reference elevation level. Thus, the residual, terrain-reduced gravity anomalies used here may be written

$$\Delta g^c = \Delta g_{BA} - \Delta g_{BA}^{ref} = \Delta g_{BA} - (\Delta g_{180} - 2\pi G\rho h_{180}) \qquad (6.1)$$

with

Δg^c: RTM anomaly, corresponds to Bouguer anomalies above $\ell=180$

Δg_{BA}:   Conventional, terrain-corrected Bouguer anomaly

Δg_{180}:   Free-air anomaly of the "Rapp-180" field

h_{180}:   Elevation from the 180 x 180 topography expansion

For the practical computations, Δg_{180} and h_{180} were computed in a $0.25° \times 0.25°$ grid, from which values at individual stations were determined by a simple bi-linear interpolation scheme.

Gravity anomalies for four different areas have been investigated. These areas will in the sequel be designated by the name of the state inside which they are located:

"OHIO":   2°x 2° lowland/moderately hilly area SW of Columbus,
             lat. 38°-40° N, lon. 85°-83° W (not identical to the Ohio
             example of the last section).

"COLORADO": 2°x 2° alpine area of the Rocky Mountains, W of Denver
             and Colorado Springs, lat. 38°-40° N, lon. 107°-105° W.

"CALIFORNIA": 2°x 2° mixed area, containing the central parts of the
             Sierra Nevada mountains and a part of the California valley,
             lat. 36°-38° N, lon. 120°-118° N.

"NEW MEXICO": 4°x 4° mountainous area, covering most of New Mexico,
             including the "White Sands" area. lat. 32°-36° N, lon.
             109°-105° W.

Except for New Mexico, these areas represent new, more detailed investigations than the results previously presented (in a somewhat different context) in Forsberg (1984). The 2°x 2° areas have been chosen to secure a sufficiently dense coverage of gravity anomalies, to allow a fairly dense grid (2'x 2.5') of gravity anomalies to be predicted. An example of the data coverage is shown in Figure 15.

The gridding procedure and analysis were similar to the method of Forsberg (1984). First, gravity anomalies were screened, keeping only one anomaly per 1'x 1' "pixel". The screened anomalies were then gridded to a 2'x 2.5' (~3.7x3.6 km) grid using a truncated collocation algorithm, where a grid point value is predicted from the five closest observations only. The dense prediction grid necessitates some caution when interpreting results for higher wave numbers: Although the data coverage for the areas is fairly dense, it is evident from Figure 15 that the data might be too sparse in parts of the areas, yielding some influence of the grid prediction method on the shape of the power spectrum at high wave numbers.

From the gridded RTM gravity anomalies power spectra, covariance functions and degree variances were constructed using the two-dimensional Fast Fourier Transform (FFT). The power spectrum is obtained from the Fourier transform by

$$\phi_{gg}(u, v) = |\Delta\tilde{g}(u, v)|^2 \qquad (6.2)$$
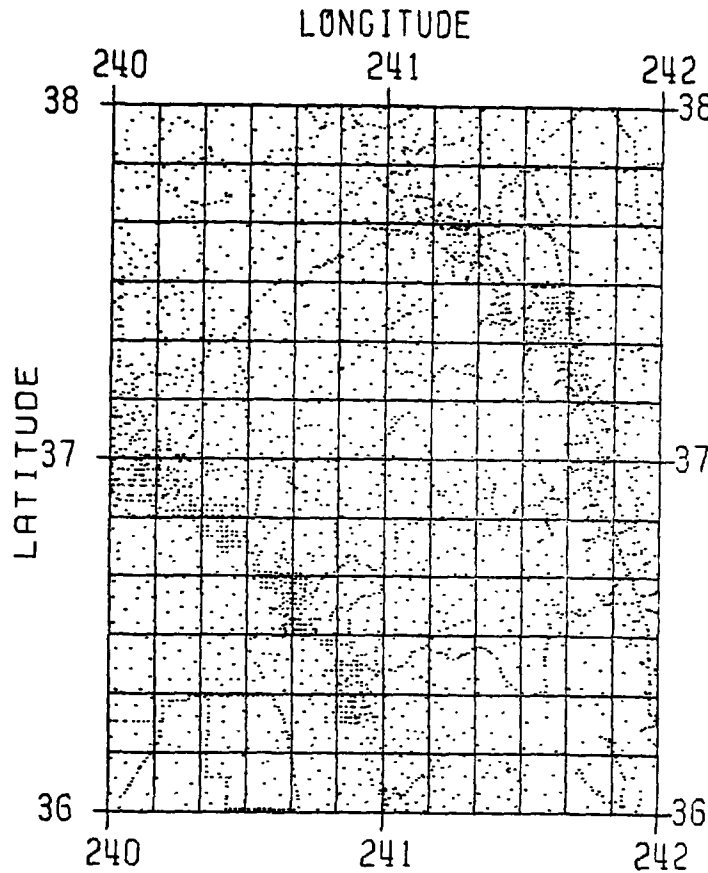
LONGITUDE

Figure 15 Gravity data coverage in the 2°x 2° area of California. The California valley is to the lower left, while the Sierra Nevada mountains run approximately NW-SE through the block. Totally 3172 1'x1' pixels contain gravity data.

and by an inverse transform the two-dimensional covariance function is obtained

$$C(x, y) = \text{Fourier}^{-1} (\phi_{gg}(u, v)) \qquad (6.3)$$

To yield "isotropic" quantities, ϕ and C were subsequently averaged along circles of constant $\omega = \sqrt{u^2+v^2}$ and $s = \sqrt{x^2+y^2}$ respectively, and from the averaged power spectrum potential degree variances were finally derived by (2.9) and (2.34):

$$\sigma_\ell = \frac{R^2}{(\ell-1)^2} c_\ell = \frac{1}{2\pi} \frac{\ell+\frac{1}{2}}{(\ell-1)^2} \phi_{gg}(\frac{\ell+\frac{1}{2}}{R}) \qquad (6.4)$$

The spectrum $\Delta\tilde{g}$ estimated using the fast Fourier transform will be affected by errors due to the finite extent of the area in question, and some suitable window filter should ordinarily be used. In the present investigation, however,

windowing turned out to be a disadvantage due to the unavoidable loss of power in the spectrum - and through the radial averaging procedure already some smoothing is done. Window filters have therefore not been applied here, resulting in somewhat "wiggling" spectra.

Results for the 2° x 2° areas are shown in Figures 16-18. Each figure shows from top to bottom graphs of σ_ℓ, $\phi_{gg}(\omega)$ and C(s) shown with a thick, solid line. The degree variances σ_ℓ are normalized and shown logarithmic, with the global degree-variance models of Kaula (3.35) and Tscherning-Rapp (3.36) also shown for comparison purposes. The power spectrum is shown logarithmic in dB (dB=10 $\log_{10}\phi_{gg}$), with unit (0 dB) 1 mgal^{2}degree^2. Wave numbers are shown in cycles/degree ($\frac{\omega}{2\pi}$), with maximum 15 cycles/degree being the Nyquist frequency for a 2' data grid. With broken lines are shown arbitrary tentative straight-line segments, with depth D determined from the slope of the line. Finally, the covariance function C(s) is shown in units of mgal^2. For reference purposes, the covariance function has been fitted with Moritz' two "basic" planar covariance functions (3.36) and (3.27): the reciprocal distance covariance (R) and the Poisson covariance (P), shown with thin line also in the power spectrum plot. The covariance functions were fitted simply by requiring variance C_0 and correlation length $x_{\frac{1}{2}}$ to match the empirical values. To illustrate possible anisotropy, the central part of the two-dimensional covariance function C(x, y) is shown as a contour plot to the right, with a contour interval of 0.2 C_0. For a perfectly isotropic process this plot would show a series of concentric circles.

(The corresponding plot of the New Mexico area, derived from a more coarse 4' x 5' anomaly grid, may be found in (Forsberg, 1984, Figure 34)).

Inspection of the power spectra shows that straight-line segments are not very conspicius. Indeed the spectra seems to be of more or less the same overall shape. The depths assigned to various parts of the power spectra in the plots must be viewed with great caution, since they are characterized by very large uncertainties. Especially for the higher wave numbers error sources due to the gridding, aliasing, and errors in the anomalies and terrain reductions play quite a substantial role in shaping the spectrum. The influence of random, uncorrelated errors in the grid points may be ascertained fairly easily using Parseval's equation (2.16): Viewing the errors as bandlimited white noise (in a frequency square of side length 2x15 cycles/degree), it follows that an error variance of 1 mgal^2 corresponds to -30 dB in Figures 16-18. Thus e.g. the tail "d ~ 1 km" of the Colorado spectrum (Figure 17) may be explained alternatively as the effect of uncorrelated gravity grid errors of variance 16 mgal^2 (~ -18 dB in the plot), not too unrealistic considering the extreme alpine topography of the area.
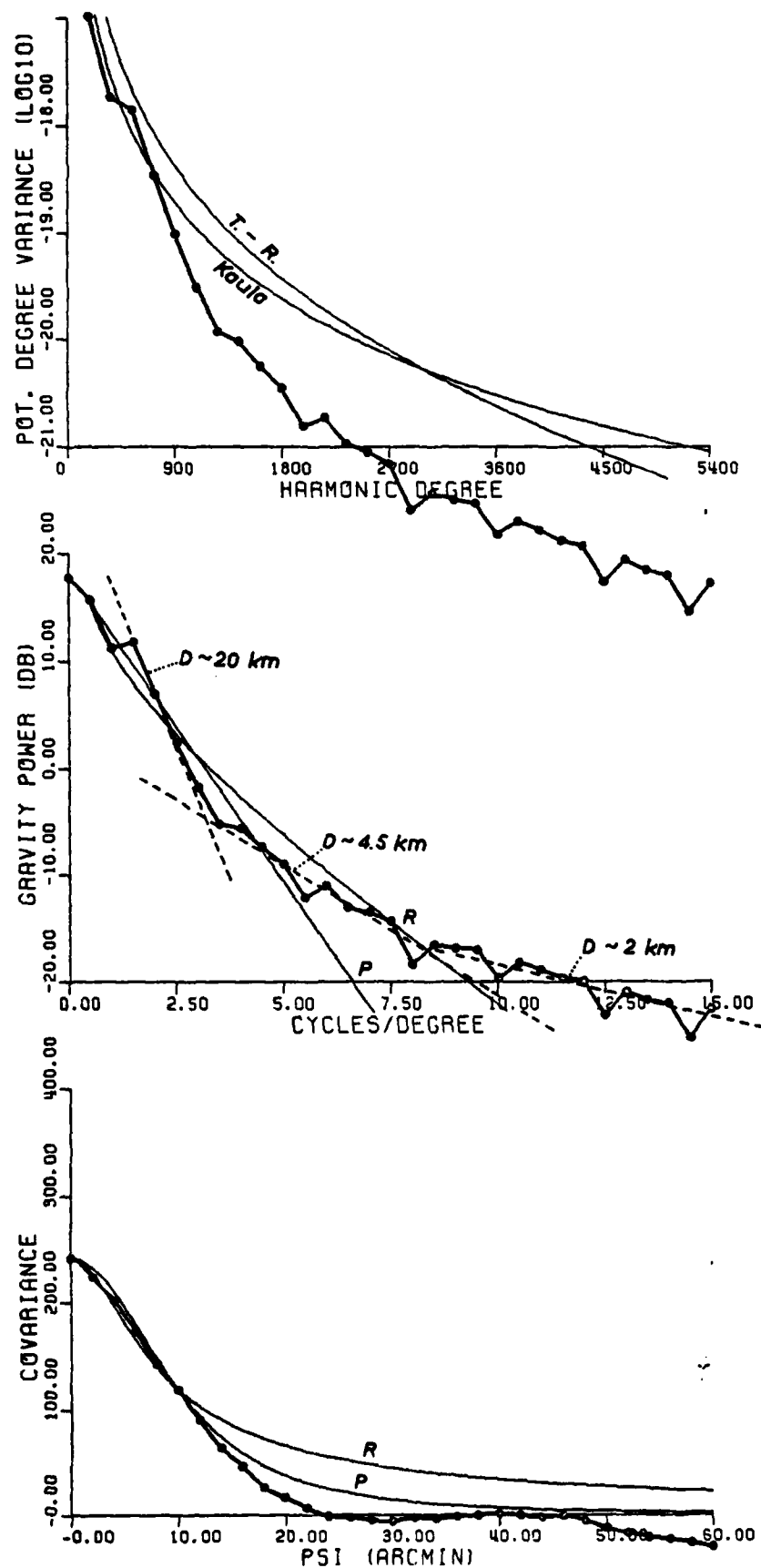
GRAVITY
LAT: 38.0 - 40.0
LON: 275.0 - 277.0
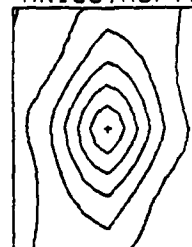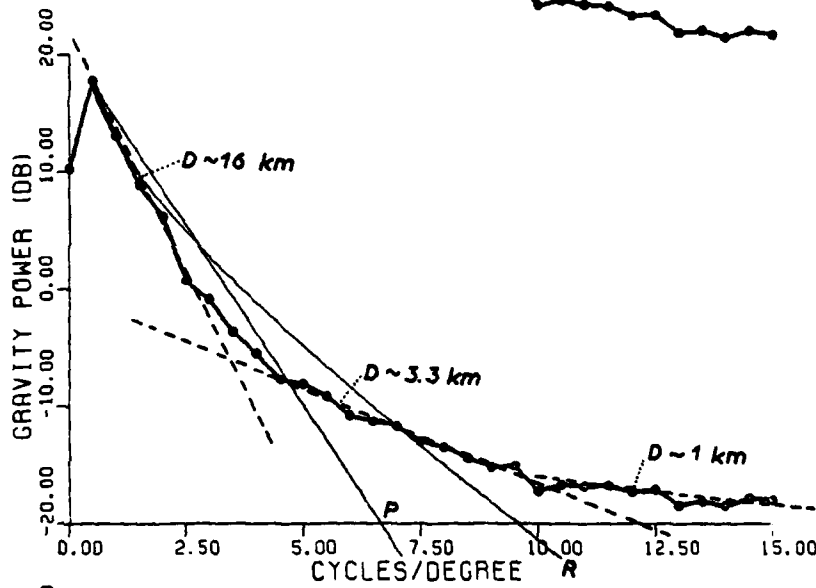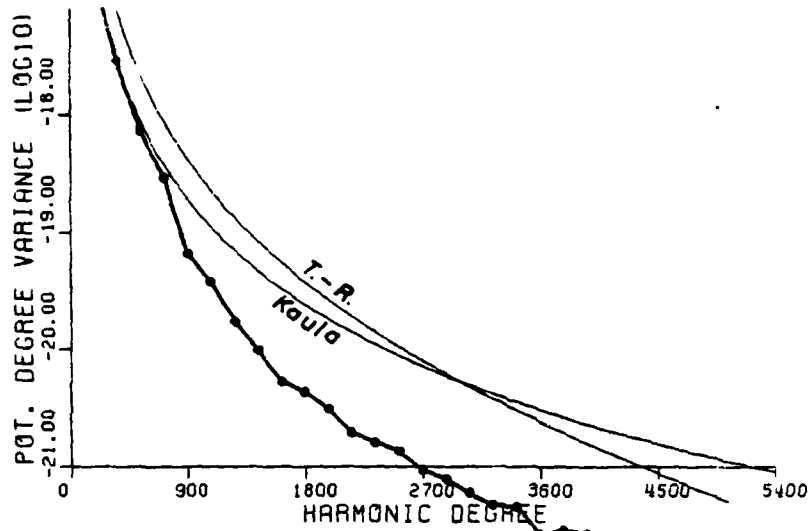SPACING: 2.0' 2.0'

ANISOTROPY:

Figure 16 Degree variances, power spectrum and covariance function for free-air gravity anomalies in a 2°x 2° area of Ohio. See text for detailed figure explanation.

GRAVITY
LAT: 38.0 - 40.0
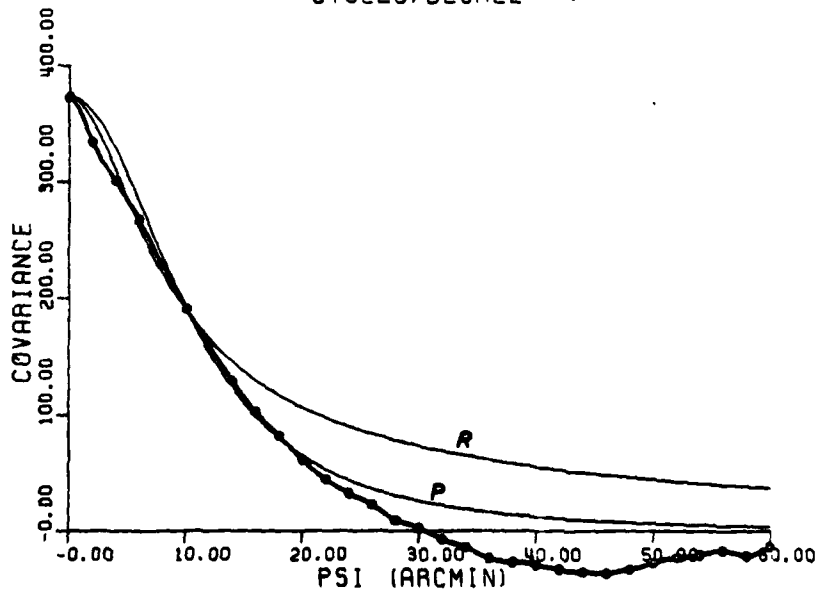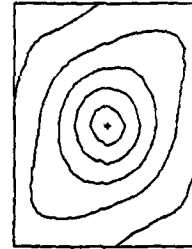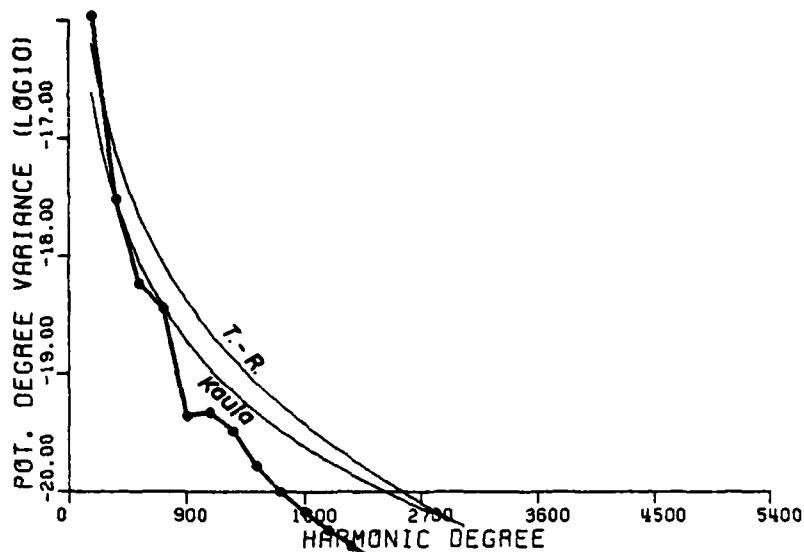LON: 253.0 - 255.0
SPACING: 2.0' 2.

Figure 17 Degree-variances, power spectrum and covariance function for residual Bouguer (RTM) anomalies in a 2°x 2° area of Colorado.

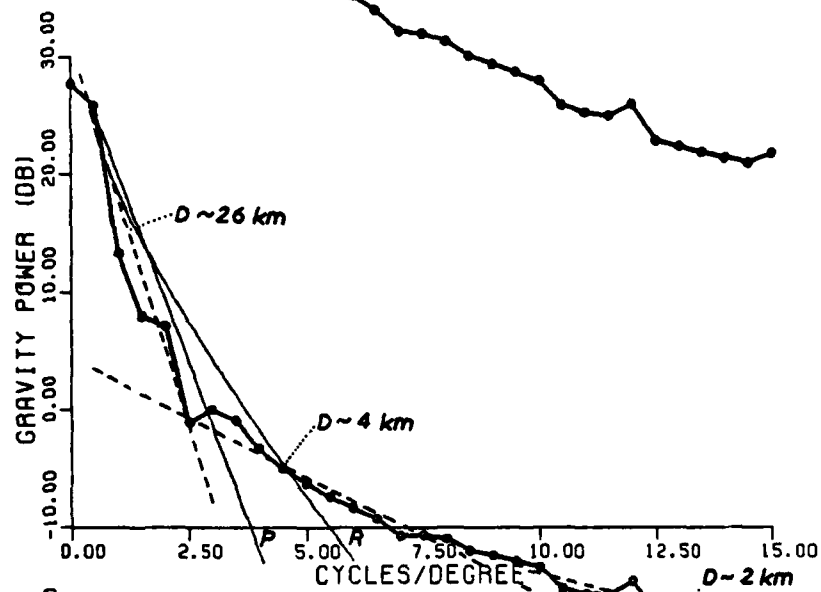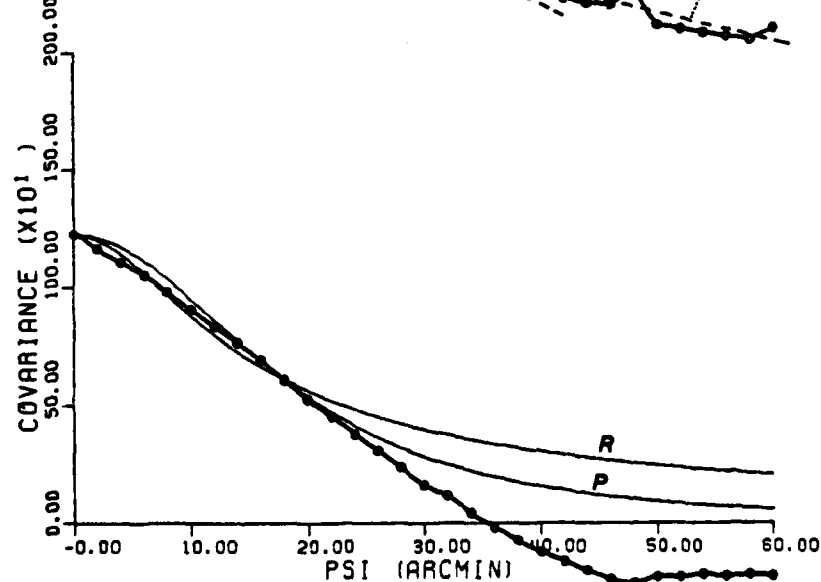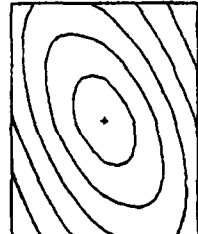Figure 18 Degree-variances, power spectrum and covariance function for residual Bouguer (RTM) anomalies in a 2°x 2° area of California.

The geophysical significance of the indicated depth values is probably limited, the depth values possibly representing merely tendencies to enhanced density variations at certain depth ranges rather than undulations of some density contrast interface. The lack of clear "layering" in the power spectrum is as earlier mentioned typical of gravity problems, opposed to many magnetic examples. The sources of the gravity field variations (besides the topography) tends to be distributed throughout the crust and upper mantle, in a random fashion quite similar for many different types of geologic settings.

Irrespectively of the geophysical interpretation of the indicated depths, they may be used to provide improved multi-layer local covariance functions of the gravity field in the respective areas. For each of the four different areas three depth values have been selected as outlined in the figures, and a total covariance function is built up by using compensated Poisson models at each of the specified depths. This gives three unknowns - the variance associated with each layer - but since the total variance is given from the data, only two free parameters are left. In addition also the compensation depth D_c may be varied, especially in order to model the apparent power left below degree 180, originating in deficiencies in the used spherical harmonic expansions of the gravity field and the topography.

The covariance models have in the present study been fitted to the power spectra using a simple interactive ad hoc technique, utilizing a graphical terminal. Each fitted power spectrum is of form (5.6)

$$\phi_{gg}(\omega) = 2\pi \sum_{i=1}^{3} \alpha_i (e^{-2\omega D_i} + e^{-2\omega D_c} - 2e^{-\omega(D_i+D_c)}) \qquad (6.5)$$

where α_i is transformed to a gravity component variance C_i by (5.12). Given the variances C_i the geoid undulation variance and gravity gradient variance are subsequently found by (5.11) and (5.16). The results are shown in Table 3 and Figure 19.

The covariance functions of Table 3 are examples of "tailored" covariance functions, applicable e.g. for optimal error studies, simulations etc. Since they have a good fit in the entire spectral range, they will be good both for geoid and second order derivative applications. The models show clearly the general feeling of gravity field variations: the geoid is sensitive to deep density variations, while second-order gradients primarily reflect shallow sources. Comparing
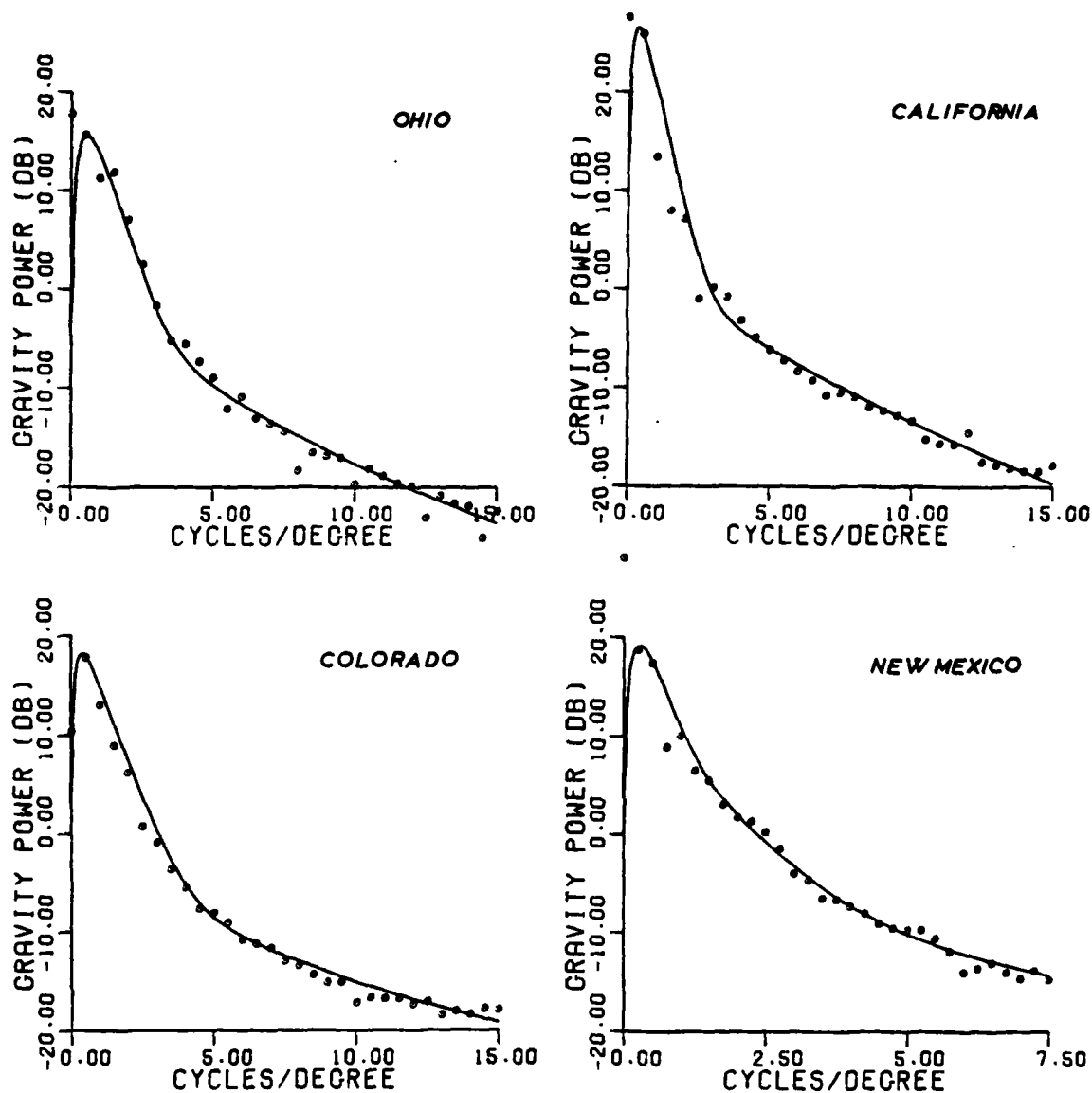
Figure 19 Examples of 3-component compensated Poisson power spectra models for the sample areas. Derived by a simple graphical fit, constrained by conservation of the total variance. Parameters listed in Table 3.

the 2°x 2° Ohio area to the previous example of Figure 12 (4°x 4° area), it is seen that quite a substantial part of the gradient variations was not resolved in the example of the last section. The increased resolution in the gravity grid of the present example thus provides for a better agreement with the torsion balance results mentioned in the last section.

Table 3

3-Layer Compensated White Noise Density Variance Models
for Residual Gravity in Sample Areas of the United States
(Topography Removed by RTM-Reduction, Except for Ohio)

Area Location	Layer Depth (km)	Gravity Variance (mgal^2)	r.m.s. variation of		
			geoid undulations (m)	gravity anomalies (mgal)	horizontal grav. gradient (E)
OHIO	2	13.3	0.02	3.6	22.3
	4.5	18.6	0.04	4.3	11.7
	20	210.3	0.37	14.5	8.9
(D_c=50 km)	total	242.1	0.38	15.6	26.7
COLORADO	1	26.1	0.02	5.1	62.6
	3.3	24.0	0.05	4.9	18.2
	16	322.8	0.54	18.0	13.8
(D_c=100 km)	total	373.0	0.54	19.3	66.6
CALIFORNIA	2	30.8	0.04	5.5	34.0
	4	46.4	0.08	6.8	20.9
	26	1148.8	1.37	33.9	16.0
(D_c=100 km)	total	1226.0	1.37	35.0	42.9
NEW MEXICO	2.5	22.9	0.04	4.8	23.4
	12	62.6	0.20	7.9	8.1
	40	112.4	0.55	10.6	3.2
(D_c=100 km)	total	197.8	0.58	14.1	25.0

With the apparent quite high similarity between the various power spectra, it is naturally then to ask the question: What is the "best" overall shape of the covariance functions in terms of the "simple" covariance models? As earlier stated, this is in general believed to be the logarithmic class of the covariance functions. That this is indeed the case may be seen from Figure 20, showing the derived degree variances on a double logarithmic plot, power functions ℓ^{-2}, ℓ^{-3} and ℓ^{-4} have additionally been plotted for reference purposes. Remembering the asymptotic forms of some of the "elementary" covariance functions of Table 1.

$$\begin{array}{lll} \text{poisson} & : & \sigma_\ell \sim \ell^{-1} \\ \text{reciprocal distance:} & \sigma_\ell \sim \ell^{-2} \\ \text{logarithmic} & : & \sigma_\ell \sim \ell^{-3} \end{array}$$

it is clear that the logarithmic types should be preferred in general. The simple planar logarithmic covariance function of Table 1 is singular, so modifications analagous to the compensated Poisson model will be needed to eliminate the influence of the low wave numbers. Alternatively, the well-known spherical Tscherning-Rapp model (3.36) may be used, with adaption to local applications obtained through a change in variance factor, Bjerhammar sphere depth and removal of lower degree-variances corresponding to the spherical harmonic reference field.

The degree variances of Figure 20 are seen to be systematically too low com-pared to Kaula's rule for the higher degrees. Kaula's rule represents a kind of global average of the actual gravity field variation, including the effects of the topography.

For a valid comparison, the topographic effects must therefore not be removed from the basic gravity grid used. In Figure 21 are shown the corresponding em-pirical degree variances for unreduced gravity data, i.e. free-air anomalies, derived from the gridded Bouguer anomalies by an inverse Bouguer reduction using elevations from detailed (0.5'x0.5') digital terrain models of the areas. Now the spread in the degree variances is much larger, reflecting the differences in terrain. The logarithmic asymptotic behaviour is still clear, and now Kaula's rule performs somewhat better, indicating e.g. that New Mexico is a quite typical area on a global basis.

The logarithmic nature of empirical gravity field covariance functions may be used for some general implications on the possible types of density distributions. If we e.g. accept the stationary thin-layered earth model, where the earth was described by a number of thin, independent layers, the total power spectrum was found in section (3.2) to be of form
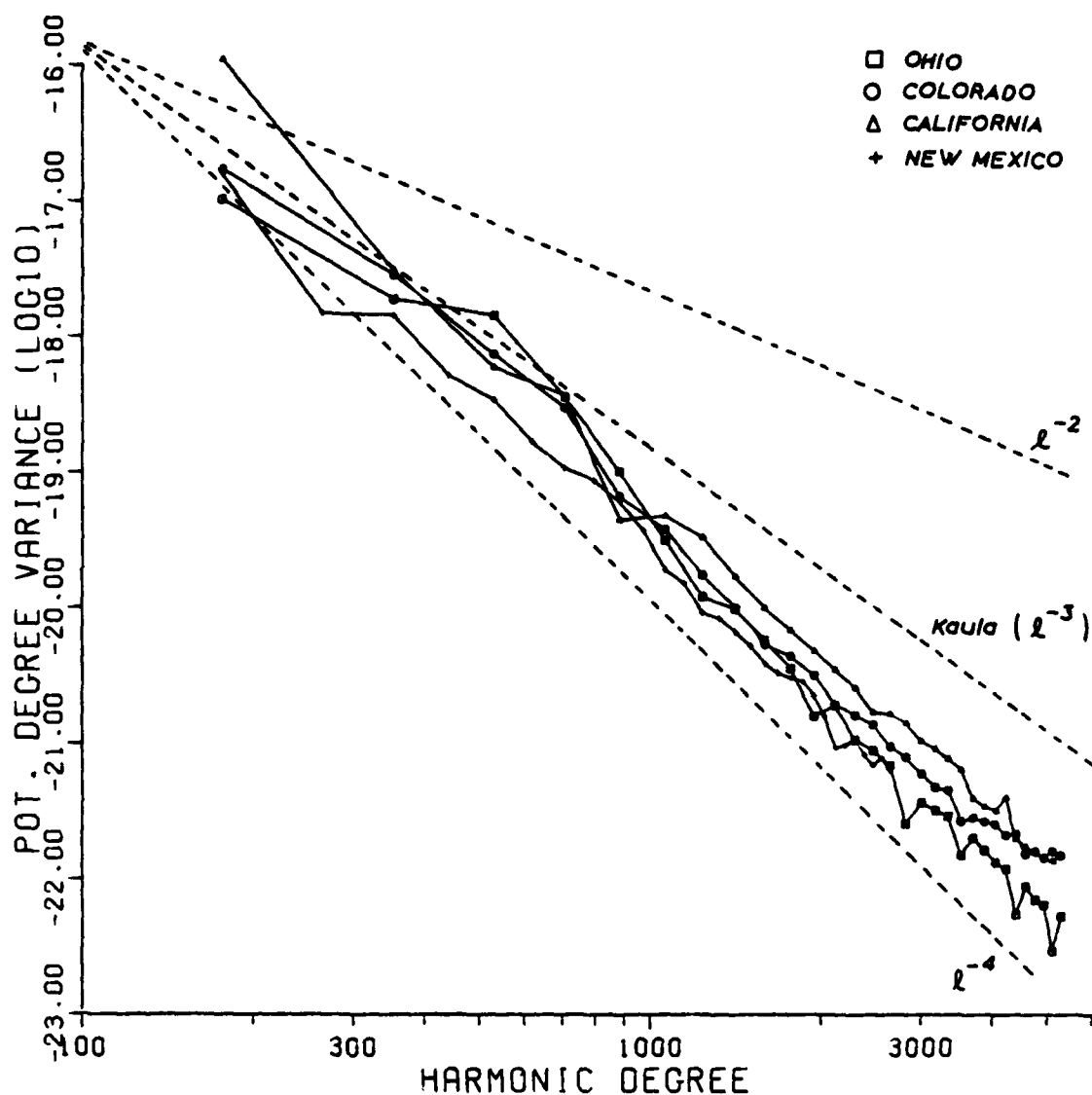
Figure 20 Empirical degree-variances for the gravity field variation in 4 U.S. sample areas. Topographic effects have been removed by an RTM-reduction corresponding to the used 180 x 180 spherical harmonic reference field (except for Ohio). Kaula's rule (3.35) shown as center broken line.
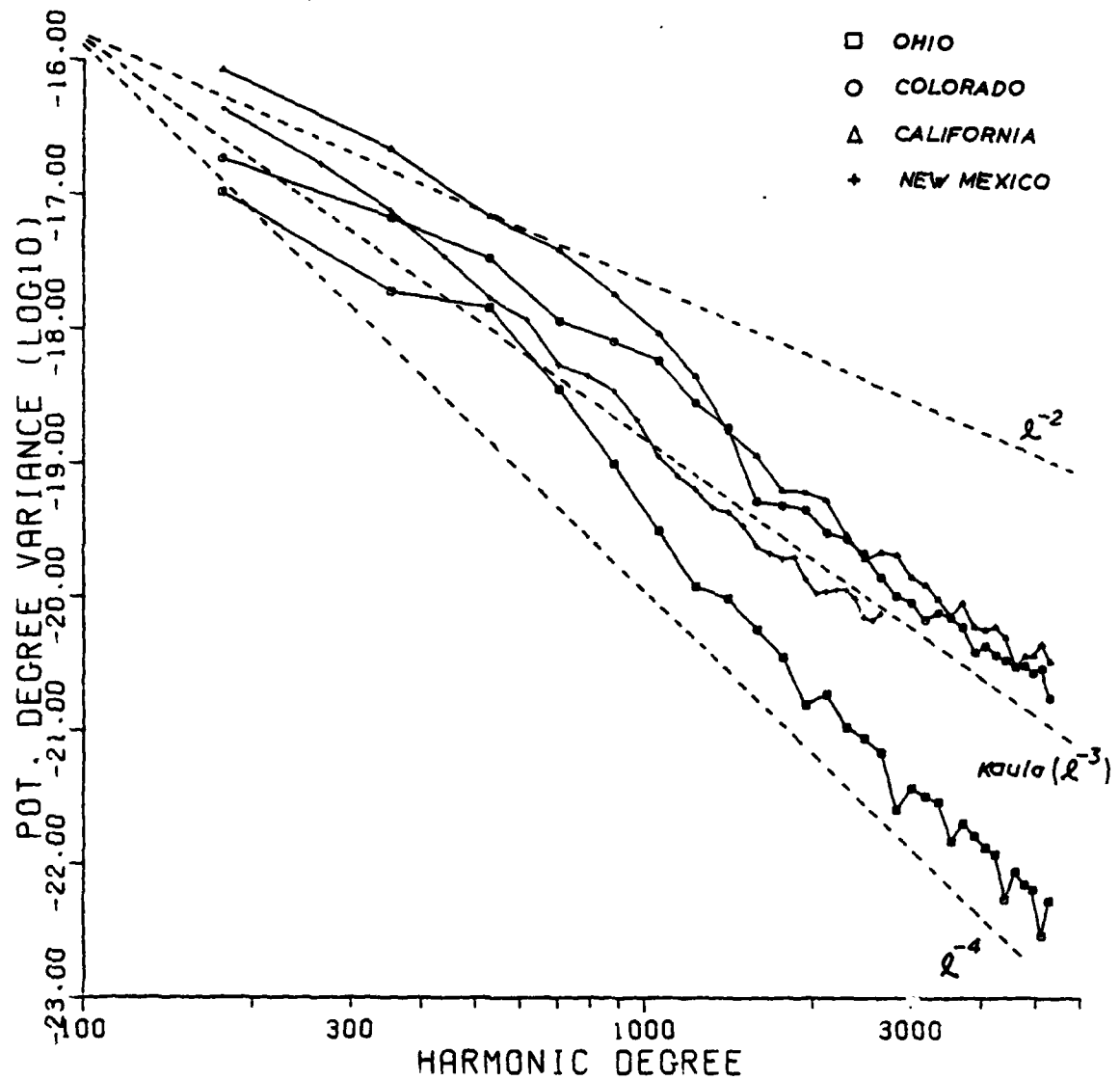
Figure 21 Empirical degree variances for the covariance sample areas, without removal of topographic effects.

$$\phi_{gg}(\omega) = \sum_i (2\pi G \Delta z_i)^2 \, \phi_{\rho\rho}^i(\omega) \, e^{-2\omega d_i} \qquad (6.6)$$

where Δz_i is the layer thickness, d_i the depth and $\phi_{\rho\rho}^i$ the density power spectrum of the layer. The form of the power spectrum for infinitely thin layers will thus be

$$\phi_{gg}(\omega) \sim \int_0^\infty \phi_{\rho\rho}(\omega, z) e^{-2\omega z} dz \qquad (6.7)$$

If the layers are assumed to be <u>identical</u>, a logarithmic power spectrum (i.e., $\phi_{gg}(\omega) \sim \omega^{-2}$) requires

$$\phi_{\rho\rho}(\omega) \sim \frac{1}{\omega} \qquad (6.8)$$

i.e. a red noise distribution, where density anomalies of large spatial extent are on the average of bigger magnitude than the density features of less extent, a quite reasonable statistical model rather than the "strong" white noise assumption.

If, on the other hand, the concept of white-noise density layers is maintained, it then follows that the density variance σ_ρ^2 must be given by an inverse Laplace transform

$$\phi_{gg}(\omega) \sim \frac{1}{\omega^2} \sim \int_0^\infty \sigma_\rho^2(z) e^{-2\omega z} dz \qquad (6.9)$$

yielding

$$\sigma_\rho^2(z) \sim z \qquad (6.10)$$

i.e., the density anomaly variance increases linearly with depth, a very unphysical result considering our general ideas of the earth's interior.

7. Summary and Conclusions

In the present report various topics relating to covariance functions and density distributions have been treated. Emphasis has been on local covariance functions, where a high degree and order spherical harmonic reference field are substracted prior to modelling and analysis. By working with the residual field, a number of simplifying assumptions may be used, such as the flat earth formulation and the identification of gravity anomalies with gravity disturbances. With these assumptions it was e.g. shown how collocation may be interpreted in a very simple fashion in terms of generalized point mass modelling.

Apart from the collocation interpetation, the various topics of the present report may be generalized easily using a spherical earth formulation. An example (which actually was part of the inspiration for the work of the present report) may be found in Sunkel (1981), who considers the white noise density layer covariances on a strictly spherical basis. For local applications, however, spherical results follow much more easily by the simple relationship existing between the planar power spectrum and the spherical harmonic degree variances.

This relationship was elaborated upon in Section 2, in addition to the most basic description needed for using the planar formulation.

In Section 3 then the relationship between the well known covariance functions (Poisson, Logarithmic etc.) and "mass bodies" characterized by white-noise distributions of density anomalies, dipole moments etc., were derived using the ensemble averaging theorem, well known to geophysicists as the method of Spector and Grant (1970). The use of the theorem opens in principle for a direct link between the shape of the power spectrum (and thus the covariance function) and depth to "disturbing" interfaces in the earth's interior.

The simple covariance functions, described e.g. as generated by a white-noise density layer, vertical mass lines etc., turned out to be themselves expressable as "gravity" effects of similar (but not the same) bodies, only at the double depth. This was used for the side remark in Section 4, the collocation interpretation. It was e.g. found simply that collocation, using the Poisson covariance function corresponds to a point mass modelling, where a point mass should be located below each gravity observation, a vertical mass line below each geoid observation point etc., at depths two times the depth to the Bjerhammar sphere.

For practical local covariance functions, in accordance with geologically reasonable density distributions, multi-layer models of independent density variations will be necessary, corresponding to different Bjerhammar sphere depths for the different constituents. In Section 5 especially the multi-layer Poisson

model was treated in some detail, and a modification based on a pseudo-isostatically "compensated white noise density" model was proposed to model the low frequency behaviour of the residual gravity field more properly. It turned out that with a perfect 180 x 180 spherical harmonic reference field, the "optimum" compensation level was only slightly deeper than the commonly accepted compensation depths of Airy isostasy. The expressions for the covariances etc. of the compensated model turned out to be very simple, since the formulas were obtained as a simple linear combination of the original Poisson formulas.

Finally, in Section 6, actual power spectra for the various sample areas were analyzed, with the primary object to detect the existence of possible disturbing interfaces. The geophysical significance of the results turned out to be questionable, an experience obtained by many geophysicists having tried to use statistical interpretation techniques for gravity anomalies. However, the inferred layer parameters are very useful in providing optimal "tailored" covariance models, and numerical values for such models were given for the different sample areas, and illustrated by providing statistics for the geoid and second order gradient variances.

Forgetting the multi-layer models, the overall shape of the covariance function turned out to be logarithmic, with degree variances decaying like ℓ^{-3} up to at least degree 5400. Kaula's rule turned out to be quite realistic for the "actual" gravity field, while the power was significantly too high when terrain-reduced data were used.

Although the statistical "covariance interpretation" techniques have not too bright prospects, I think it could be of interest for future studies to take more sample areas, especially areas in geologic settings where a "white-noise layer" description would be expected to have some validity, e.g. for describing undulations in salt/sediment interfaces in salt dome provinces (like e.g. the Gulf coast of Texas or northern Jutland, Denmark). In such cases important information on the very local variability and stationarity of the "detailed" covariance functions could additionally be derived. A prerequisite for such studies would be a very dense gravity coverage, combined with power spectrum estimation techniques yielding reliable estimates even for small sample areas, inside which the "layering" assumption is reasonably valid.

References

Dorman, L.M. and B.T.R. Lewis: Experimental isostasy 1. Theory of the determination of the earth's isostatic response to a concentrated load. JGR, 75, no. 17, 1970.

Engelis, T., C.C. Tscherning and R.H. Rapp: The precise computation of geoid undulation differences with comparison to results obtained from GPS. Preprint, submitted to GRL, 1984.

Forsberg, R.: A study of terrain reductions, density anomalies and geophysical inversion methods in gravity field modelling, Department of Geodetic Science and Surveying, Report No. 355, The Ohio State University, 1984 (in print).

Gradstein, I.J. and M.Y. Ryshik: Table of integrals, series, and products. Academic Press, New York, 1965.

Heiskanen, W.A. and H. Moritz: Physical geodesy. Freeman, 1967.

Jekeli, C.: An investigation of two models for the degree variances of global covariance functions. Department of Geodetic Science and Surveying, Report No. 275, The Ohio State University, 1978.

Johansen, H.K. and Sørensen, K.: Fast Hankel Transforms. Geophysical Prospecting, 27, pp. 876-901, 1979.

Jordan, S.K.: Statistical model for gravity, topography and density contrasts in the earth. Journal of Geophysical Research, 83, No. B4, pp. 1816-1824, 1978.

Langel, Estes and Mead: Some methods in geomagnetic modelling applied to the 1960-1980 epoch. NASA Technical Memorandum 83868, 1981.

Moritz, H.: Advanced physical geodesy. Herbert Wichman Verlag, Karlsruhe, 1980.

Nash, R.A. and S.K. Jordan: Statistical geodesy - an engineering perspective. Proc. IEEE, 66, No. 5, 1978.

Papoulis, A.: Systems and transformations with applications in optics. McGraw-Hill, New York, 1968.

Petersen, L.B.: A statistical analysis of potential fields using a vertical cylinder and a dike. Geophysics, 43, No. 5, pp. 943-53, 1978.

Phillips, R.J. and K. Lambeck: Gravity fields of the terrestrial planets: Long wavelength anomalies and tectonics. Rev. Geoph. Space Phys. 18, No. 1, pp. 27-76, 1980.

Rapp, R.H.: The earth's gravity field to degree and order 180 using Seasat altimeter data, terrestrial gravity and other data. Department of Geodetic Sience and Surveying, Report No. 322, The Ohio State University, 1981.

Rapp, R.H.: Degree variances of the earth's potential, topography and its iso-static compensation. Bull. Geod., 56, pp. 84-94, 1982.

Spector, A. and F.S. Grant: Statistical models for interpreting aeromagnetic data. Geophysics, 35, No. 2, pp. 293-302, 1970.

Sunkel, H.: Point mass models and the anomalous gravity field. Department of Geodetic Science and Surveying, Report No. 328, The Ohio State University, 1981.

Tscherning, C.C. and R.H. Rapp: Closed covariance expressions for gravity anom-alies, geoid undulations and deflections of the vertical implied by anomaly degree variance models. Department of Geodetic Science, Report No. 208, The Ohio State University, 1974.

Tscherning, C.C.: Covariance expressions for second and lower order derivatives of the anomalous potential, Department of Geodetic Science, Report No. 225, 1976.

END

FILMED

3-85

DTIC